# GYPSUM–HYDROBORACITE ASSOCIATION IN THE SIJES FORMATION (MIOCENE, NW ARGENTINA): IMPLICATIONS FOR THE GENESIS OF Mg-BEARING BORATES

FEDERICO ORTÍ[1] AND RICARDO N. ALONSO[2]
[1] *Universitat de Barcelona, Facultat de Geologia, Zona Universitària de Pedralbes, 08071 Barcelona, Spain*
*e-mail: orti@natura.geo.ub.es*
[2] *Universidad Nacional de Salta–CONICET, Buenos Aires, 177, 4400 Salta, Argentina*
*e-mail: ralonso@impsat1.com.ar*

ABSTRACT: **This paper deals with sedimentologic and diagenetic aspects of the evaporitic facies of the Sijes Formation (Miocene, central Andes, NW Argentina), which contains the largest known hydroboracite reserves in the world. In outcrop, the sulfate minerals are secondary gypsum and minor anhydrite, and the borate minerals are hydroboracite with subordinate inyoite and colemanite, and some ulexite. In the Monte Amarillo Member of the Sijes Formation it is possible to distinguish two coeval, shallow lacustrine subbasins, in which the gypsum accumulated in the margins and the hydroboracite in the centers, the intermediate zones being characterized by mixed gypsum–hydroboracite layers. In the depositional sequence, primary gypsum (gypsarenite) and syndepositional anhydrite, in association with limited amounts of calcium borates (colemanite, inyoite) precipitated first, followed by hydroboracite (calcium/magnesium borate). Alternations of gypsum and hydroboracite layers also formed. Hydroboracite is mainly a primary mineral, although it replaced some gypsum under synsedimentary conditions. The formation of colemanite, which occurred during early diagenesis, is linked to the precipitation of calcium sulfates (gypsum and anhydrite), whereas inyoite coexists with both calcium sulfates and magnesium-bearing borates. Transformations among the various borate minerals during burial diagenesis were not detected. Primary gypsum was transformed into anhydrite from early diagenesis to moderate burial diagenesis. The boron source of these deposits seems to be related to the volcanic/hydrothermal activity in the central Andes during the Miocene.**

## INTRODUCTION

Borate minerals accumulated in lacustrine settings are an interesting case of evaporite precipitation. In many Neogene deposits formed in these lakes, the calcium borates are prevalent, in particular colemanite (Table 1). These colemanite deposits, some of which have considerable economic interest (Kistler and Helvaci 1994), have no analogs in modern environments. This lends support to the interpretation of a secondary origin for many ancient colemanite deposits (Smith and Medrano 1996). In other colemanite deposits, however, a number of factors suggest a primary origin, including: well established stratigraphic relations, insufficient burial depth, depositional cyclicity, and textural and petrographic evidence (Helvaci 1995; Helvaci and Ortí 1998).

A similar situation applies to the presence of Mg-bearing borate minerals in Neogene deposits, for which modern analogs are scarce or inappropriate. Moreover, the Mg-bearing borates in the ancient formations usually occur only as subordinate minerals, though not as dominant phases. The Miocene Sijes Formation of NW Argentina contains the most important deposits of hydroboracite—a low hydrated Ca/Mg borate—known in the world. As in the case of several calcium borates, there are no modern lacustrine deposits of hydroboracite to compare with (the hydroboracite deposits of the Inder region seem to be related to Permian salts of marine origin; Aristarain and Hurlbut 1972). This suggests that hydroboracite is mainly diagenetic and would probably result from dehydration of a preexisting phase. Nevertheless, some of the earlier interpretations (Alonso 1986; Aristarain 1991) of the hydroboracite in the Sijes Formation regarded a primary origin as very probable. This paper describes the Neogene hydroboracite deposits of the Monte Amarillo Member of the Sijes Formation, in which abundant gypsum is associated with the borate minerals. This case is of special interest for the following reasons: (1) the origin of Mg-borates is a complex subject (Crowley 1996); (2) the close association between hydroboracite and gypsum allows us to elucidate the genetic relations between borates and sulfates in the ancient formations (little literature is available on this subject; Ortí et al. 1998); and (3) these relations will bring a better understanding of the origin of colemanite (Helvaci and Ortí 1998).

## GEOLOGIC AND STRATIGRAPHIC SETTING

The Miocene Sijes Formation, which accumulated in the Pastos Grandes Neogene basin (Alonso 1986), is located in the area of the salar Pastos Grandes and the Sijes Sierra (Fig. 1A), in the southern Puna region (Salta province, NW Argentina). This arid region is the segment, located between 24° and 26° S latitude, of the Puna/Altiplano plateau, which is a structural unit dominating the central Andes with an internal drainage and an average altitude of 3700 m (Isacks 1988; Vandervoort et al. 1995). The plateau was formed in a compressional orogen during late Cenozoic times (Allmendinger 1986; Jordan et al. 1983). In the southern Puna, a combination of east-trending volcanic chains and north-trending uplifted, reverse-fault-bounded structural blocks created numerous basins that formed the site of active nonmarine sedimentation during Neogene times (Jordan and Alonso 1987). The Neogene basin fill in the southern Puna consists of thick (up to 5 km) sequences of continental evaporites and alluvial clastics with subordinate tuffaceous deposits (Alonso et al. 1991). Outcrops of Neogene evaporitic strata occur within or adjacent to modern depositional surfaces, where evaporite saline pans (salars) occupy the lowest parts (Igarzábal 1979, 1991; Jordan and Alonso 1987). In the southern Puna region, evaporites older than Miocene are absent.

The Pastos Grandes Neogene basin (Fig. 1B) contains sediments up to 2000 m thick that were deposited on a variety of fluvial, alluvial, and saline-lake environments. The main lithostratigraphic units (Alonso 1986, 1992; Vandervoort 1993, 1997) are indicated in Figure 2A. The Pozuelos Formation (Miocene) includes two depositional members, the Clastic Member and the Evaporite Member, the latter being mainly made up of rock salt. The Sijes Formation (Miocene) has four members; three of them are composed of a fine-grained siliciclastic, tuffaceous, and chemical-evaporitic

TABLE 1.—*Borate minerals cited in the text.*

| | |
|---|---|
| CALCIUM BORATES | |
| Inyoite | $Ca_2B_6O_{11}\cdot 13H_2O$ |
| Meyerhofferite | $Ca_2B_6O_{11}\cdot 7H_2O$ |
| Colemanite | $Ca_2B_6O_{11}\cdot 5H_2O$ |
| Priceite | $Ca_4B_{10}O_{19}\cdot 7H_2O$ |
| Howlite | $Ca_4Si_2B_{10}O_{23}\cdot 5H_2O$ |
| SODIUM OR SODIUM-BEARING BORATES | |
| Ulexite | $NaCaB_5O_9\cdot 8H_2O$ |
| Probertite | $NaCaB_5O_9\cdot 5H_2O$ |
| Borax | $Na_2B_4O_7\cdot 10H_2O$ |
| MAGNESIUM OR MAGNESIUM-BEARING BORATES | |
| Hydroboracite | $CaMgB_6O_{11}\cdot 6H_2O$ |
| Inderborite | $CaMgB_6O_{11}\cdot 11H_2O$ |
| Inderite | $Mg_2B_6O_{11}\cdot 15H_2O$ |
| Kurnakovite | $Mg_2B_6O_{11}\cdot 15H_2O$ |
| Pinnoite | $MgB_2O_4\cdot 3H_2O$ |

JOURNAL OF SEDIMENTARY RESEARCH, VOL. 70, NO. 3, MAY, 2000, P. 664–681
 1073-130X/00/070-664/$03.00

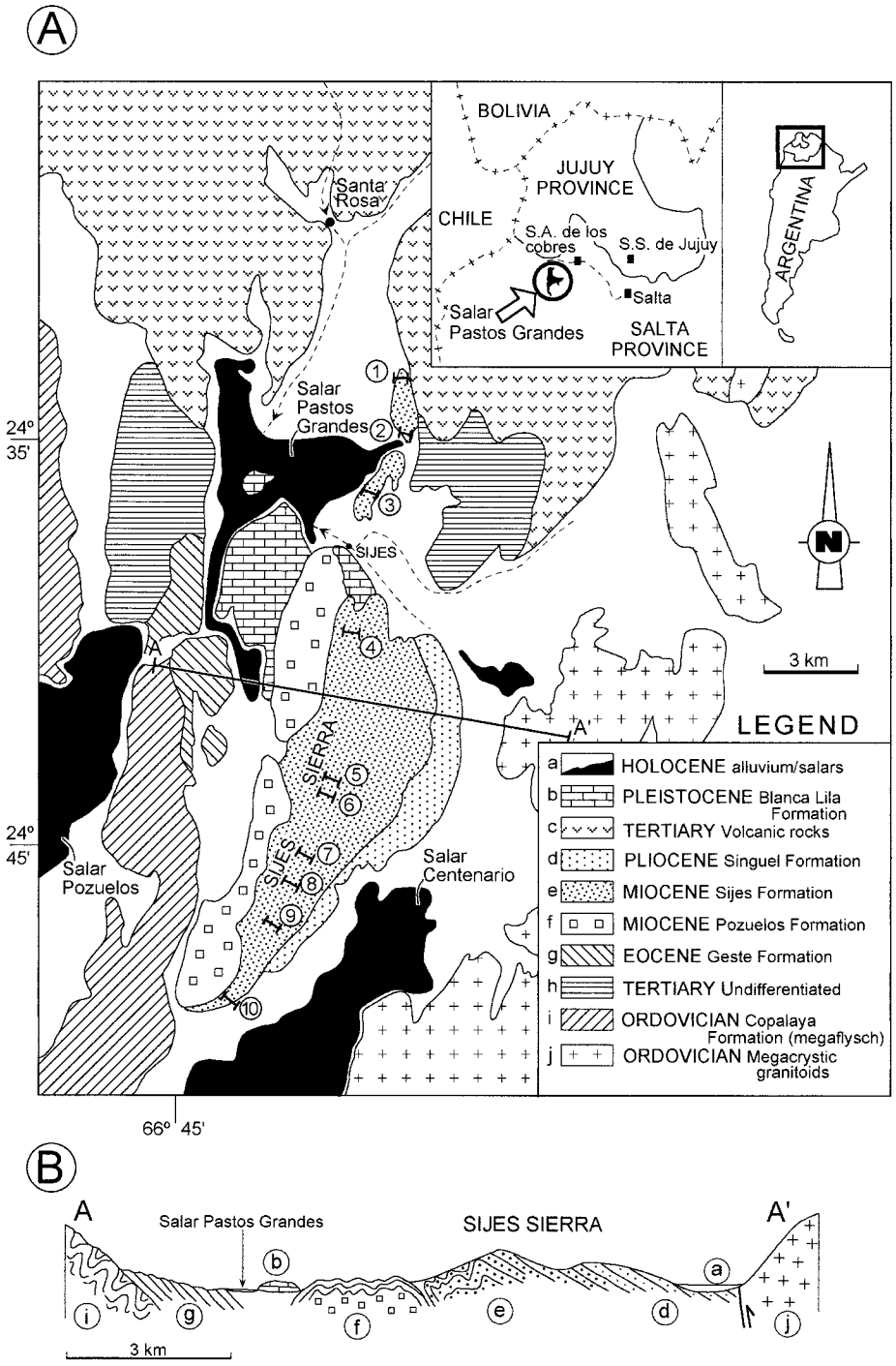


FIG. 1.—**A**) Geological map of the Pastos Grandes basin in the Sijes Sierra (simplified from Alonso 1992, fig. 1). The position of the sections studied corresponding to the most important borate districts and mines along the Sijes Sierra is indicated: 1, Santa Elvira; 2, Santa Elena; 3, Santa Rosa; 4, Ona; 5, Apalacheana; 6, Monte Azul; 7, Monte Amarillo; 8, Sorpresa; 9, Monte Marrón; 10, Anita. **B**) Geological section (A–A′) across the Sijes Sierra (simplified from Alonso 1986, plate 12, fig. 3). The location of this section is indicated in part A.

nature (the Monte Amarillo Member, the Monte Verde Member, and the Esperanza Member), and one member has a coarse-grained siliciclastic character (the Conglomerate Member). The Blanca Lila Formation (Pleistocene) is made up of claystone and evaporites. The lithology, thickness, chronostratigraphy, radiometric age ranges, and major unconformities of these units are given in Figure 2A.

### *Borate Content of the Stratigraphic Units and Hydroboracite Subbasins*

The borate content of the various units of the Pastos Grandes basin was studied by Alonso (1986) (Fig. 2B). At the top of the Pozuelos Formation, halite and gypsum layers contain mineable inyoite and ulexite. The Sijes Formation has the largest borate content, and in the Sijes Sierra (Fig. 1A) there are borate occurrences in the three evaporite-bearing members of this formation. The existence of these borate occurrences coincides with the paleogeographic center of this basin during the accumulation of the Sijes Formation. The sedimentation of the borate and gypsum deposits of this unit was coeval with intense volcanic activity, as indicated by the prevalence of pyroclastic layers intercalated in the stratigraphic section. Alonso and Viramonte (1990, 1993) attributed the origin of boron in the boratiferous Tertiary formations and recent salars in the Puna region to volcanic

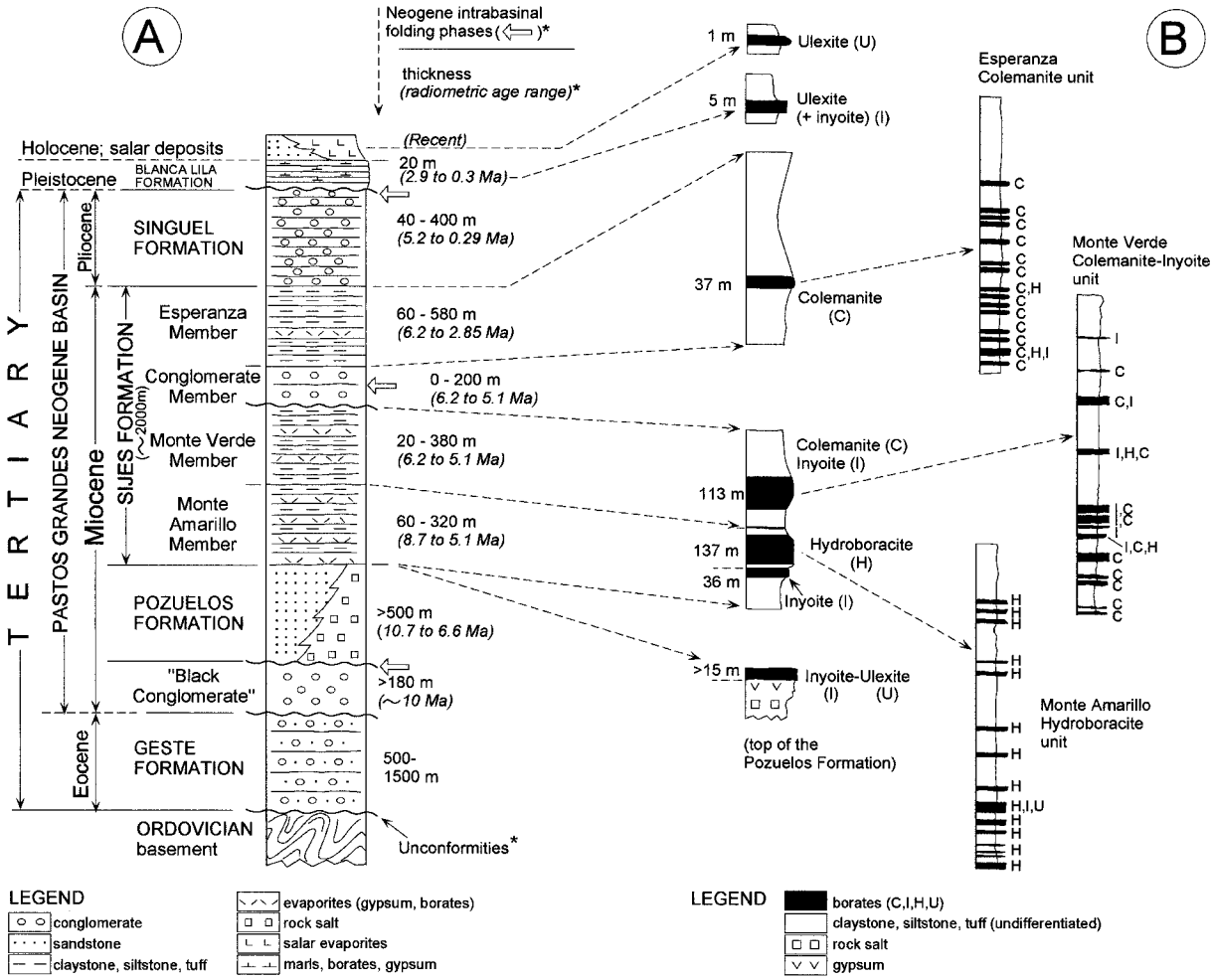


FIG. 2.—**A**) General stratigraphic section of the Tertiary and Quaternary sediments in the Pastos Grandes basin and the Sijes Sierra area (adapted from Alonso 1986 and Vandervoort 1993). (*), data taken from Vandervoort (1993) (radiometric age in millions of years, Ma); the Neogene unconformities are related to phases of intrabasinal compression and folding. **B**) Borate units and occurrences. The thickness of the borate units in the type sections of the various members is taken from Alonso (1986). Mineral symbols: C, colemanite; I, inyoite; U, ulexite; H, hydroboracite.

activity on the basis of the currently active, boron-rich hydrothermal springs, and the numerous indices of this activity in the central Andes during the Holocene. The presence of arsenous sulfides (realgar, orpiment) in the Sijes Formation also suggests a hydrothermal origin for arsenic.

The type section of the Monte Amarillo Member, which is 317 m thick, contains an inyoite unit 36 m thick at the base, which is overlain by a hydroboracite unit 137 m thick (Fig. 2B). This hydroboracite unit has variable amounts of inyoite and ulexite. Gypsum layers are ubiquitous in the Monte Amarillo Member. Samples of two tuff levels located close to the base and at the top of this section were dated as 6.81 ± 0.18 and 6.25 ± 0.15 Ma, respectively, which indicates a depositional period of about $6 \times 10^5$ years for the Monte Amarillo Member during the Upper Miocene (Alonso 1986). The type section of the Monte Verde Member, which is 378 m thick, contains an inyoite–colemanite unit 113 m thick (Fig. 2B), with subordinate hydroboracite. Lateral gradations between colemanite/inyoite and hydroboracite layers are observed. Gypsum layers are widely distributed in the member. The type section of the Esperanza Member, which is 580 m thick, contains a colemanite unit 37 m thick, with small amounts of inyoite, hydroboracite, and ulexite. Gypsum is subordinate in this member (Fig. 2B).

Two major hydroboracite subbasins can be distinguished in the Monte Amarillo Member: (A) The Monte Amarillo hydroboracite subbasin, which comprises the borate districts to the south of the Sijes village (districts nos. 4 to 10, Fig. 1A). The most important of them is the Monte Amarillo district (no. 7), which has been exploited since 1985. This district is located at an altitude of 3900 m and lies near the paleogeographic center of the Monte Amarillo subbasin. (B) The Santa Rosa hydroboracite subbasin, which includes the borate districts to the north of the Sijes village (districts nos. 1 to 3, Fig. 1A). The most important of them is the Santa Rosa district (no. 3), which is located at an altitude of 3900 m. This subbasin occupies a marginal position with respect to the Monte Amarillo subbasin. In these subbasins, the hydroboracite layers are fine-grained, light brown, and difficult to break with the hammer (Fig. 4A). Because of these characteristics, they had for long time been confused with limestones, until they were identified by Catalano (1926). More recently, these hydroboracite deposits have been studied by several authors. Rusansky (1985) carried out a chemical and petrographic investigation in the Santa Rosa district; Alonso (1986) made a general study and interpretation of the various hydroboracite facies; and Aristarain (1991) presented a detailed mineralogical study of the hydroboracite occurrences.

## MATERIALS AND METHODS

Field work, sampling, stratigraphic observations, and facies analysis were carried out in outcrop and in open cuts in the Sijes Formation. Ap-

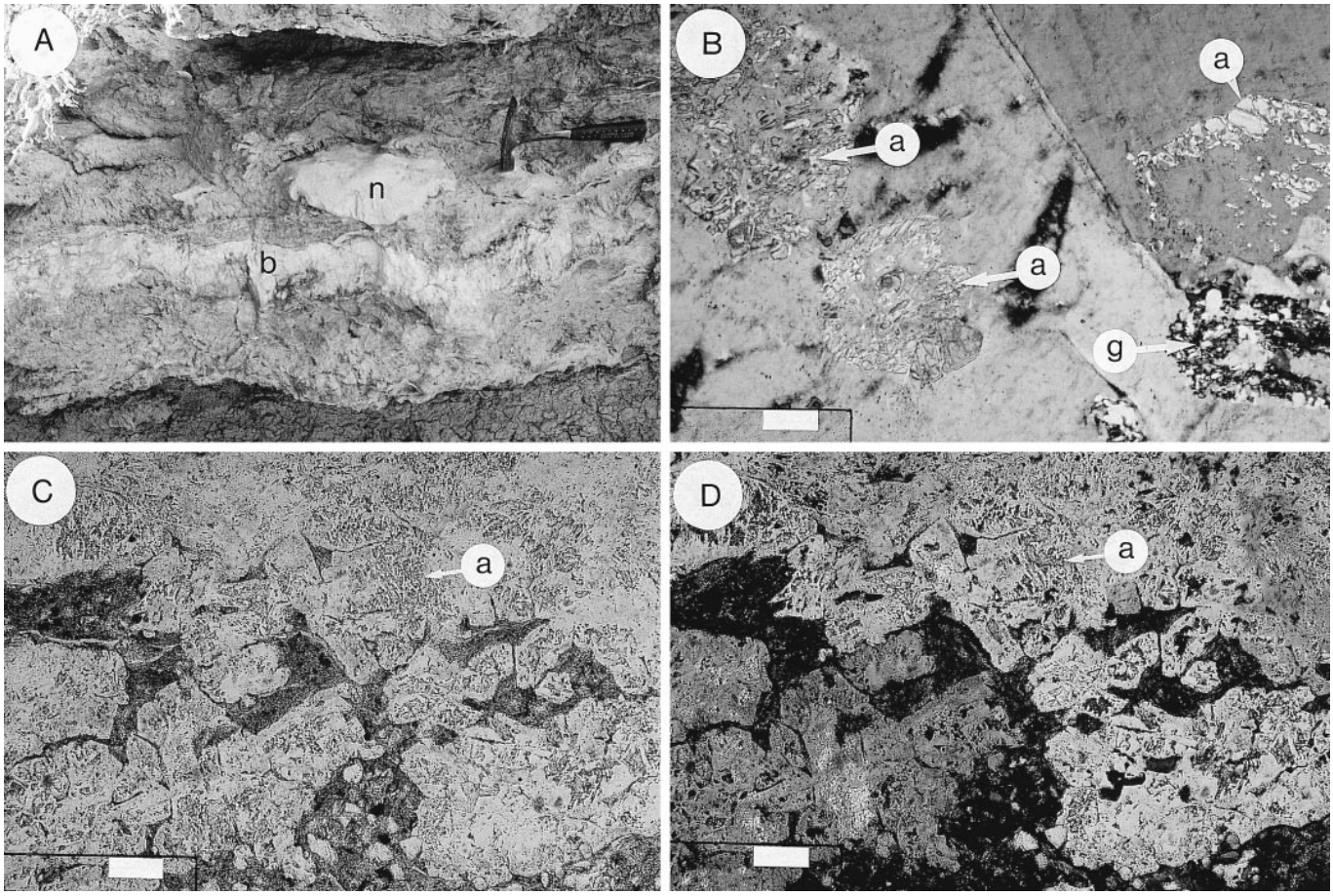


FIG. 3.—Gypsum facies, and photomicrographs of gypsum and anhydrite fabrics. **A**) Banded massive, and nodular facies of gypsum formed by alabastrine secondary gypsum (in white). Banded massive (b) facies forms a continuous bed in the central part of the picture. The flattened nodule (n) suggests that compaction within a soft host sediment occurred during early diagenesis. The gray material is a mixture of secondary gypsum and clay. Hammer for scale. **B**) Pseudomorphs after (precursor) euhedral, gypsarenite crystals partly preserved in anhydrite (a), and in fine-grained, alabastrine secondary gypsum (g). Two crystals of megacrystalline secondary gypsum cement all these pseudomorphs. Bar: 0.16 mm. **C, D**) Secondary gypsum pseudomorphs after (precursor) subhedral to euhedral gypsarenite crystals. Precursor crystals can be seen both in normal light (C) and crossed nicols (D); abundant anhydrite relics (a) can be distinguished. Two large, anhedral crystals of secondary gypsum containing all the precursors are seen in part D. Bar: 0.16 mm.

proximately one hundred samples of gypsum, hydroboracite, colemanite, inyoite, anhydrite, and carbonate were polished and studied petrographically in large (5.5 cm × 4.5 cm) thin sections. The mineralogy of these samples was systematically identified by XR diffraction analysis.

## THE MONTE AMARILLO MEMBER: EVAPORITE PETROLOGY

In the Monte Amarillo Member, the sediments interlayered with the evaporitic precipitates are siliciclastics (claystone, siltstone, sandstone) and pyroclastics (ash fall, tuff). Clay minerals are mainly illite and smectite, mixed with minor interlayered minerals. Tuff layers have an andesitic composition (Alonso 1986) and are dominated by crystalline components (crystal tuff) with subordinate lithic and vitric clasts; crystal fragments are quartz, microcline, sanidine, andesine, biotite, hornblende, muscovite, and calcite. Pyroclastic (tuff) layers are *in situ* deposits that alternate with the evaporitic precipitates. Siliciclastic layers commonly include volcaniclastic components that were transported into the basin. A few carbonate beds made up of calcitic—and subordinate dolomitic—mudstone are interlayered with the evaporitic precipitates. There is no evidence of the presence of halite, or of sulfates other than calcium sulfates, in the surface and subsurface in the three members of the Sijes Formation. A maximum burial of about 1500 m is estimated for the Monte Amarillo Member (Vandervoort 1993).

### *Gypsum and Anhydrite*

The most abundant gypsum is secondary, i.e., it results from near-surface hydration of precursor anhydrite. The main facies distinguished in these secondary gypsum rocks are: laminated, banded, banded massive, massive, nodular, and enterolithic (Fig. 3A). In the laminated gypsum, corrugated, algal-like morphology is common, as well as wavy ripples overprinted on the gypsum laminae. Petrographically, identification of the secondary gypsum is based on the presence of (1) porphyroblastic, alabastrine, and megacrystalline fabrics, (2) anhydrite relics, and (3) pseudomorphs after (precursor) primary gypsum crystals (Shearman et al. 1972; Ortí 1977). These pseudomorphs are preserved uncommonly as anhydrite (Fig. 3B), and generally as secondary gypsum (Fig. 3C, D). Locally, these pseudomorphs show palisade fabric (subvertical arrangement of crystals). The characteristics of the secondary gypsum facies and the fabrics of secondary gypsum and anhydrite are summarized in Table 2. Diagenetic gypsum is scarce, being limited to (1) some macroscopic crystals that are either isolated or grouped into small rosettes, (2) satin spar veins of gypsum, and (3) coarse crystalline gypsum that poikilitically cements the non-evaporitic matrix.

**Interpretation.**—Given the presence of abundant pseudomorphs after fine-grained, primary gypsum, the laminated and banded facies can be interpreted as gypsarenites (sand-size gypsum precipitates) deposited in shallow-water environments. Gypsum crystals with palisade fabric suggest

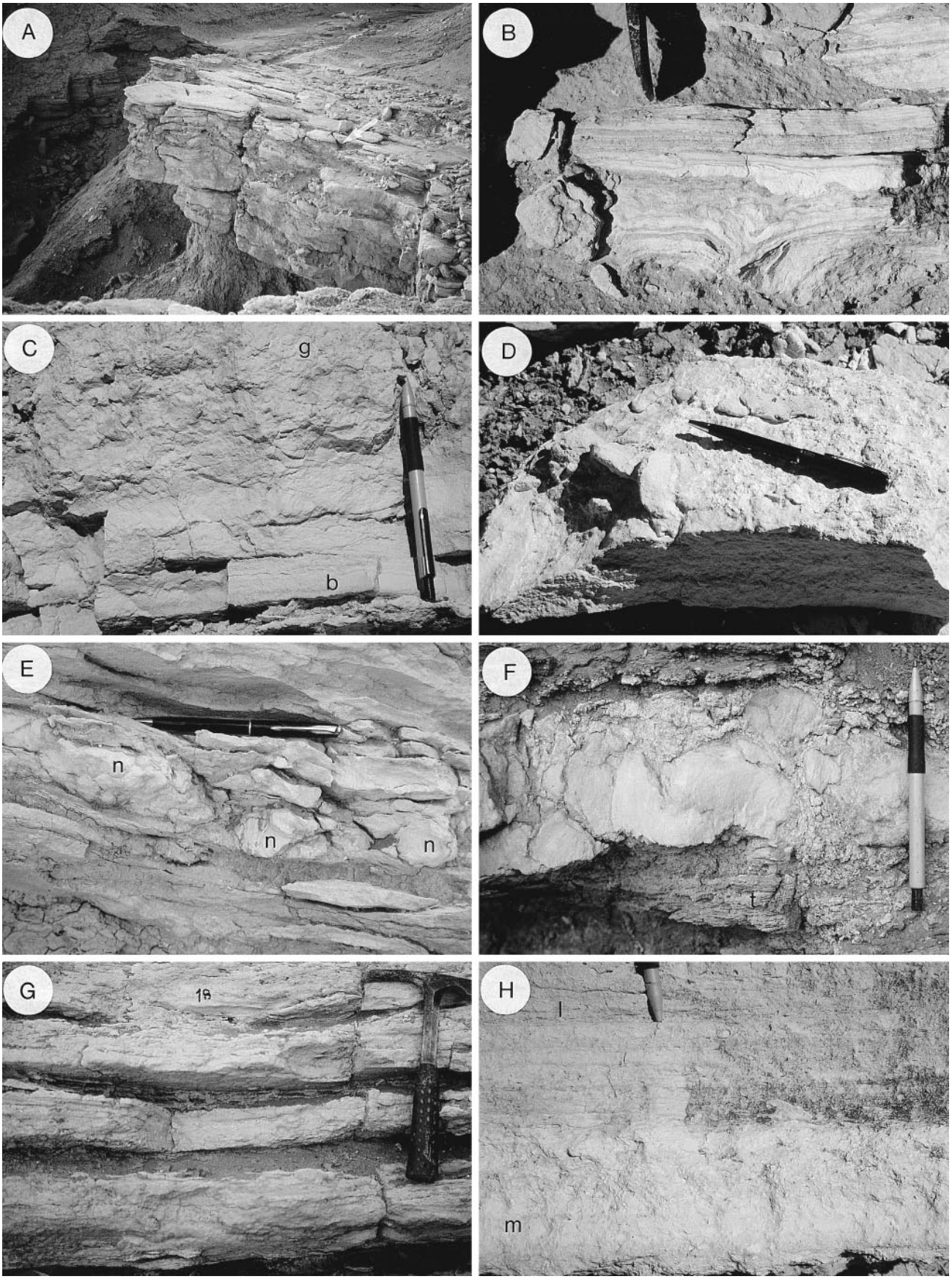

TABLE 2.—*Facies and crystalline fabrics of gypsum and anhydrite (Fig. 3).* **(1)** *characteristics* **(2)** *sedimentary structures* **(3)** *pseudomorphs* **(4)** *interpreted original facies.*

| |
|---|
| **SECONDARY GYPSUM** |
| **Laminated, banded gypsum** |
| **(1)** Laminae (up to 1 cm thick) and bands (1–10 cm thick) have parallel, undulated or corrugate (algal-like) morphology. **(2)** Wavy ripples can be superimposed on the lamination. **(3)** Shapes of the precursor crystals (pseudomorphs) are euhedral, subhedral and lenticular. Size oscillates from 10–100 $\mu$m; in general, pseudomorphs are homometric, but less commonly, size is very variable, some of the pseudomorphs reaching up to 3 mm in length. Zoned pattern in these precursors is common. Packing of these precursors is relatively open, and interpenetration is little developed; a few palisade (subvertical) arrangements in the pseudomorphs (up to 5 mm in size) are observed. **(4)** Alternation of (common) gypsarenite laminae, and (rare) palisade gypsum laminae. |
| **Massive, banded massive gypsum** |
| **(1)** Layers (>10 cm thick) are devoid or almost devoid of inner structure. **(2)** Poorly defined burrow morphology, which is reinforced by some ferruginization. **(3)** Similar to those in the laminated facies, although palisade gypsum is absent. **(4)** Banded to massive gypsarenite. |
| **Nodular, enterolithic gypsum** |
| **(1) (2)** Nodules have diameters ranging from <1 cm (micronodules) to >50 cm (meganodules). Enterolithic gypsum forms contorted beds up to 20 cm thick. Morphology of the nodules is variable, most commonly flattened. Meganodules are rare. **(3)** Pseudomorphs are absent. **(4)** Displacive, nodular anhydrite grown under synsedimentary conditions. Some nodules formed as displacive gypsum in the hydroboracite layers. |
| *Crystalline fabrics of secondary gypsum* |
| Alabastrine (microcrystalline, fibrous, with undulose extinction) and porphyroblastic (crystals with planar to interpenetrated boundaries, and perfect to undulose extinction) fabrics are prevalent; megacrystalline (crystals > 1 cm in length) fabric is less common. Anhydrite relics are common. Abundant pseudomorphs after primary gypsum (gypsarenite) are present. Microcrystalline celetite is commonly observed. |
| **GYPSUM CEMENT** |
| *Satin spar veins* are composed of gypsum fibers arranged perpendicular to fractures or stratification joints. *Coarse crystalline gypsum* is formed by anhedral, crystalline plates that poikilitically cement sandstones and tuffs. *Gypsum rosettes* are formed by displacive/cementing macrolenticular gypsum. In general, all these gypsum precipitates formed from calcium-saturated circulating waters during late diagenesis (exhumation) at the time of final rehydration of precursor anhydrite into secondary gypsum (a similar process has been described for the satin spar veins by El Tabakh et al. 1998). In a few cases, however, the satin spar veins are formed by secondary gypsum, thus indicating the existence of an anhydrite precursor. |
| **CRYSTALLINE FABRICS OF ANHYDRITE** |
| Anhydrite is mainly made up of fine grained, equant, euhedral crystals forming granular fabrics (prismatic fabrics are absent); size varies from 40 to 100 $\mu$m; rhombic and pseudohexagonal sections are common. Rare recrystallization features are observed, such as anhedral to poikilitic plates (up to a few millimeters in length). Discrete crystals of anhydrite pseudomorphing individual (precursor) crystals of gypsarenite are common. |

TABLE 3A.—*Facies of hydroboracite (Fig. 4).* **(1)** *characteristics* **(2)** *sedimentary structures* **(3)** *pseudomorphs* **(4)** *replacive/displacive origin.*

| |
|---|
| **Laminated, banded hydroboracite** |
| **(1)** Laminae (up to 1 cm thick) and bands (1–10 cm thick) of very fine grained hydroboracite, usually with parallel geometry. **(2)** Mudcracks, bird tracks, and raindrops are found. Convoluted lamination and other synsedimentary structures indicating deformation of soft sediments are common. **(3)** Hydroboracite pseudomorphs after gypsarenite crystals are observed in the gypsum-hydroboracite alternations. |
| **Massive hydroboracite** |
| **(1)** Layers > 10 cm thick, without inner structure. **(2)** Footprints of birds are found. |
| **Globular hydroboracite** |
| **(1) (2)** Bands and layers with inner structure formed by (1) interlocking, globular or lump-like masses (these masses are commonly <1 cm long but always <5 cm long), and poorly defined nodules; and (2) hydroboracite matrix. The tops and bases of these bands and layers have a nodulose morphology. **(3)** Pseudomorphs are absent. |
| **Intraclastic, brecciated hydroboracite** |
| **(1) (2)** Clast-supported horizons (up to 10 cm thick) composed of hydroboracite clasts (up to 1 cm long) embedded in a hydroboracite matrix. The intraclasts are rarely larger, very sharp and matrix-poor, resembling thin intraformational breccias. Gradation between this facies and the globular facies exists. Fenestra-like and laminoid fenestra-like structures can be seen under the microscope. **(3)** Pseudomorphs are absent. |
| **Nodular hydroboracite** |
| **(1) (2)** Nodules (up to 10 cm in diameter) and micronodules (<1 cm in diameter) are formed by fine grained hydroboracite, in general. Nodular morphology varies from subspherical to flattened, and irregular. Some nodules are curved and elongated (they have a flowed appearance) and can correspond to load casts and flame structures; some of them display macrocrystalline fibrous texture (''fibrous nodules''). Some subspherical nodules rarely have an inner, macrocrystalline radial texture. Isolated hydroboracite nodules can also be embedded in other lithologies, such as gypsum, sandstone, and tuff. Nodular horizons resembling enterolithic layers are rare. **(3)** Pseudomorphs are absent. **(4)** Nodules can both displace and replace the host sediment (tuff, gypsum). |
| **Lenticular masses of hydroboracite** |
| **(1) (2)** Masses up to 1 m long are intercalated within siliciclastic and tuff layers. These masses can grade into discrete nodular morphologies, or can form discontinuous horizons. **(4)** These are displacive masses. |
| **Tuffaceous hydroboracite** |
| **(1) (2)** A perfect gradation exits between tuff layers with only little hydroboracite cement, and hydroboracite layers in which only the remnants of some pyroclastic components are observed. Clasts of hydroboracite as well as gypsum crystals are mixed with the vitric clasts in tuff layers. Laminated to massive stratification characterizing the tuff deposits is present. Fenestra-like microstructures are common. **(3)** Hydroboracite pseudomorphs after lenticular gypsum are present locally. **(4)** Hydroboracite commonly cements and replaces the tuffaceous components, in particular the crystal fragments. |

some episodes of competitive growth. The massive facies and the banded massive facies can be interpreted as gypsarenites deposited along the margins of lakes in very shallow-water to emergent conditions (Ortí 1997). The nodular and enterolithic facies represent interstitial growth of anhydrite under synsedimentary conditions during subaerial exposure (sabkha/playa setting; Shearman 1966). In contrast, the laminated and banded massive gypsum layers, which are not affected by nodular growths, could have been transformed into anhydrite mainly during burial diagenesis. Nevertheless, pseudomorphs after primary gypsum exhibit euhedral shapes, loose packing, boundaries very little disturbed by pressure solution, and minor mechanical reorientation (Fig. 3C), suggesting that (1) compaction of the gypsarenite was limited, and (2) its transformation into anhydrite occurred from early diagenesis to only moderate-burial diagenesis.

### *Hydroboracite*

Hydroboracite layers can be very pure or can be mixed in all proportions with other sediments. Locally, these layers contain abundant arsenous sulfides (realgar, orpiment). The main facies are the following: laminated and banded (Fig. 4B), massive, globular (Fig. 4C), intraclastic/brecciated (Fig. 4D), nodular and enterolithic (Fig. 4E, F), lenticular masses, and laminated alternations of gypsum and hydroboracite (Table 3A). In these facies hydroboracite can display wavy ripples, mudcracks, footprints of birds, and raindrops locally (Alonso 1986). Also, hydroboracite alternates with claystone and tuff (Fig. 4G), and is commonly present as mixed, tuffaceous–hydroboracitic layers (Fig. 4H). Aside from these major facies, hydroboracite can occur as a cement of sandstone layers. In general, hydroboracite is very fine grained (Fig. 5A). The most common fabrics (Table 3B) oscillate from microfibrous to fibrous and exhibit massive or fluid-like arrangements (Fig. 5B, C). Other hydroboracite fabrics are microprismatic to prismatic (Fig. 5D), aligned-prismatic, microgranular, and in radial aggregates. Various cementing fabrics are observed, including rim, blocky mosaic, and drusy mosaic textures (Fig. 5E). In the mixed tuffaceous–hydroboracitic layers, some particular cementing fabrics, such as fenestra-like (Fig. 5F), and laminoid fenestra-like (Fig. 5G) are distinguished; other fabrics are replacive to the tuff (Fig. 5H).

**Interpretation.**—The laminated, banded, and massive facies represent primary, subaqueous precipitates (hydroboracite mud). The associated sedimentary structures indicate that the lake environment was very shallow. However, some thick hydroboracite layers devoid of sedimentary structures other than fine lamination could be attributed to deeper lacustrine environments. The intraclastic/brecciated facies correspond to breakage and accumulation of fragments of partly indurated hydroboracite laminae. This

←

FIG. 4.—Hydroboracite facies. **A**) Layers of hydroboracite (total thickness of about 4 m) alternating with thin clay horizons. Hydroboracite unit in the Monte Amarillo district. Hammer for scale (arrow). **B**) Laminated and banded facies of hydroboracite. The lower half of the layer is affected by synsedimentary deformation and displays convoluted lamination. Hammer for scale. **C**) Banded facies (b; lower half of the layer) and globular facies (g; upper half of the layer) of hydroboracite. Note the gradual transition between the two facies. Pencil: 14 cm. **D**) Intraclastic facies of hydroboracite as seen at the base of a (reversed) block of a hydroboracite layer. **E**) Nodular (n) facies of hydroboracite intercalated between banded facies of the same mineral. Pen: 15 cm. **F**) Enterolithic-like facies in a hydroboracite layer intercalated between laminate tuff (t; in gray). **G**) Alternation of banded hydroboracite layers (in white) and thin horizons of tuff. **H**) Hydroboracite as a cement of pyroclastic layers: the lower half is formed by a massive (m) hydroboracite layer in which a few pyroclastic components remain; this layer grades upward into a laminated (l), hydroboracite-cemented tuff. Pen for scale.

TABLE 3B.—*Crystalline fabrics of hydroboracite (Fig. 5).*

- ***Fibrous fabrics.*** These are hydroboracite fabrics formed by microfibers (5–50 $\mu$m long) or fibers (50 $\mu$m–0.3 mm long, locally up to 1 mm long) that exhibit various arrangements: massive, fusiform, fascicular, flowed, and roughly spherulitic. The hydroboracite in these fabrics can be mixed in all proportions with clayey, tuffaceous, or calcareous matrix; the fibers and fiber groups are commonly affected by bending and flowed deformation as original growth features. In some flowed arrangements, the fibers can be oriented normal to bedding. Some fibrous fabrics made up of very pure white hydroboracite resemble ulexite.
- ***Prismatic fabrics.*** These are hydroboracite fabrics formed by microprismatic (5–50 $\mu$m long) or prismatic crystals (50 $\mu$m–0.5 cm long) which exhibit decussate, spherulitic, aligned, and flowed arrangements. In some laminated alternations between hydroboracite and gypsum, the hydroboracite laminae show a coarse (prisms up to 1 mm long), prismatic-aligned fabric. In other cases, prismatic veins of the satin spar type can be identified under the microscope. Some hydroboracite laminae are formed by fine microprisms (10–15 $\mu$m long).
- ***Microgranular fabrics.*** These are hydroboracite fabrics formed by tiny (5–50 $\mu$m), equant crystals, which resemble the micritic texture of the carbonate rocks.
- ***Radial fabrics.*** These are crystalline aggregates formed by very coarse (up to 1 cm long), fibrous to prismatic crystals; these aggregates can form individualized nodules. Several cleavage systems in dense arrangements are observed in the sections normal to the prisms.
- ***Blocky mosaic and drusy fabrics.*** These are fabrics composed of equant to prismatic crystals (30 $\mu$m–2 mm long) forming discrete areas within the various fibrous and prismatic fabrics. In these blocky and drusy areas, the hydroboracite crystals are transparent, and rarely twinned. These fabrics commonly cement a preexisting secondary porosity (formed by dissolution) within other hydroboracite fabrics. In few cases, coarse crystalline (>2 mm in length), blocky mosaic fabrics are tectonically induced recrystallization products of a precursor, fine grained hydroboracite fabric, in association with some folding and faulting in these deposits.
- ***Anhedral fabrics.*** Some fractures and lamination joints are cemented by (1) subhedral to anhedral hydroboracite crystals, and (2) anhedral, long (several mm) and narrow hydroboracite plates.
- **Cementing to replacive fabrics in tuff and sandstone.** Various fabrics of hydroboracite can cement and replace the vitric matrix and the crystal fragments in tuff layers. Commonly, a *rim fabric* (prismatic hydroboracite) surrounds and replaces the vitric clasts. Other fabrics, such as *blocky mosaic* and *drusy mosaic*, can cement the tuffaceous clasts. Very typical is the *fenestrae-like fabric*, in which hydroboracite shows microscopic, cementing structures of the fenestra and fenestra-laminoid geometry characterizing some limestones; these structures are composed of microfibers, prisms, and microgranular crystals of hydroboracite, and were usually formed by early fracturing, shrinkage, and brecciation of the vitric matrix. In sandstone layers, hydroboracite occurs as a cement; moreover, very irregularly shaped to nodular masses of this mineral can replace the clastic components.

fracturing could occur during episodes of very shallow to emergent conditions and desiccation, as well as in paleosol-related settings. The globular facies, which grades laterally into the intraclastic facies, could have had a similar origin. Hydroboracite nodules displaying elongated (flattened, fluid-like) morphology suggest the influence of some mechanical effect, such as load casting. Rare enterolithic-like structures indicate a subaerial setting, as is the case of the calcium sulfates in the vadose–capillary zone (Shearman 1966). The formation of large, lenticular masses of hydroboracite is the result of discontinuous, displacive growth within a soft sediment. Precipitation of hydroboracite as a cement in the siliciclastic and tuffaceous layers, with or without associated replacement, seems to be an early diagenetic event, given that these mixed layers are commonly intercalated between pure hydroboracite layers or grade into them. The fine-grained, fibrous or prismatic fabrics of hydroboracite are primary features, and the strong deformation and flowed appearance exhibited by the fibrous fabrics seem to be an original growth characteristic. Thus, significant recrystallization affecting these fabrics was not found. Moreover, there is no evidence of pseudomorphs after a precursor borate, suggesting that the hydroboracite is mainly a primary precipitate.

### *Alternations of Gypsum and Hydroboracite*

Alternations between gypsum and hydroboracite laminae are present in the transition from gypsum units to hydroboracite units (Fig. 6A, B). In the gypsum laminae, a fine-grained hydroboracite matrix commonly cements and partly replaces (Fig. 6C) the precursor gypsarenite crystals (currently secondary gypsum pseudomorph; primary gypsum preserved is rare). Furthermore, micronodules of hydroboracite can be found displacing or replacing the gypsum laminae. In the hydroboracite laminae, two main types of pseudomorphs after interstitially grown (precursor) gypsum are present: Type I corresponds to hydroboracite pseudomorphs after euhedral, lenticular or tabular gypsum crystals (Fig. 6D). Many of theses pseudomorphs are thin, curved, or slightly deformed, being composed of fine-grained hydroboracite (Fig. 6E). Others, however, are well formed and made up of parallel prisms of hydroboracite that project from the boundaries to the cores; the cores of the pseudomorphs are commonly occupied by secondary gypsum bearing anhydrite relics (Fig. 6F). The parallel arrangement of the prisms suggests replacement of the (precursor) gypsum along the main cleavage plane (010). Type II corresponds to secondary gypsum pseudomorphs after equant to prismatic, commonly zoned (precursor) gypsum crystals. These pseudomorphs are located in the uppermost parts of the hydroboracite laminae, and they grade to the secondary gypsum pseudomorphs forming the overlying gypsum lamina. Pseudomorphs of type II crosscut and replace type I pseudomorphs (Fig. 6E). This fact suggests that type II pseudomorphs postdate those of type I.

**Interpretation.**—Regular alternations between gypsum laminae and hydroboracite laminae suggest a shallow environment, where the fine-grained, soft hydroboracite mud adapted to the morphologies of the laminated gypsarenites. The prevalent microcrystalline or fibrous textures of hydroboracite suggest a primary origin for these alternations in which precipitating conditions oscillate continuously from gypsum to hydroboracite. In the gypsum laminae, the hydroboracite matrix appears to have precipitated interstitially within the open fabric of the (precursor) gypsarenite under synsedimentary conditions. This precipitation, together with associated partial replacement of (precursor) gypsum crystals (Fig. 6C), occurred during the sedimentation of the overlying hydroboracite lamina. In the hydroboracite laminae, type I pseudomorphs seem to correspond to (precursor) gypsum crystals that grew interstitially in the hydroboracite matrix when the borate concentration of the brine was relatively low. It appears that these crystals were very soon replaced by the hydroboracite matrix. The deformation of the pseudomorphs that are formed by fine-grained hydroboracite (Fig. 6E) suggests that the replacement process took place in a soft matrix under synsedimentary conditions. However, when this replacement occurred as a growth of prisms along the cleavage planes, the pseudomorphs remained undeformed and consistent; in general, this mechanism was less penetrative, and many pseudomorphs had a mixed hydroboracite–gypsum composition. Presumably, in these mixed pseudomorphs, the anhydrite replacement of the gypsum postdates the partial hydroboracite replacement. These pseudomorphs changed to hydroboracite–anhydrite during burial, and to hydroboracite–secondary gypsum in final exhumation (Fig. 6F). Type II pseudomorphs seem to correspond to (precursor) gypsum crystals that grew interstitially toward the tops of the hydroboracite laminae during precipitation of the overlying gypsarenite. We conclude that the precursor gypsum crystals of the two pseudomorphic generations formed under syndepositional conditions (Fig. 7).

→

FIG. 5.—Photomicrographs of hydroboracite fabrics. **A**) Very fine-grained, microprismatic hydroboracite forming thinly laminated facies. Laminae are deformed near the contact with tuff material (lower left corner). Crossed nicols. Bar: 0.32 mm. Size of the hydroboracite microprisms varies between 10 and 30 $\mu$m. **B**) Fibrous fabric; groups of fibers display various arrangements (fan-shaped, fusiform, fascicular). Crossed nicols. Bar: 0.08 mm. **C**) Fibrous fabric exhibiting bending and flowage deformation. Crossed nicols. Bar: 0.32 mm. **D**) Prismatic hydroboracite. In the lower right corner, a group of prisms oriented normal to the photographic plane shows several exfoliation systems. Normal light. Bar: 0.32 mm. **E**) Rim (r) and drusy mosaic (d) fabrics of hydroboracite cementing a (preexisting) pore in tuff (t; dark material). Crossed nicols. Bar: 0.08 mm. **F**) Fenestra-like fabric of microgranular (m) hydroboracite cementing a vitric matrix (dark material) in tuff. To the right, a fibrous (f) fabric of hydroboracite can be seen. Normal light. Bar: 0.16 mm. **G**) Laminoid fenestra-like fabric of prismatic hydroboracite (f) cementing partly broken tuff laminae (t). Normal light. Bar: 0.08 mm. **H**) Spherulites and rims of fibrous to prismatic hydroboracite cementing and replacing crystal fragments in tuff (see the quartz crystal in the center; q). Crossed nicols. Bar: 0.08 mm.

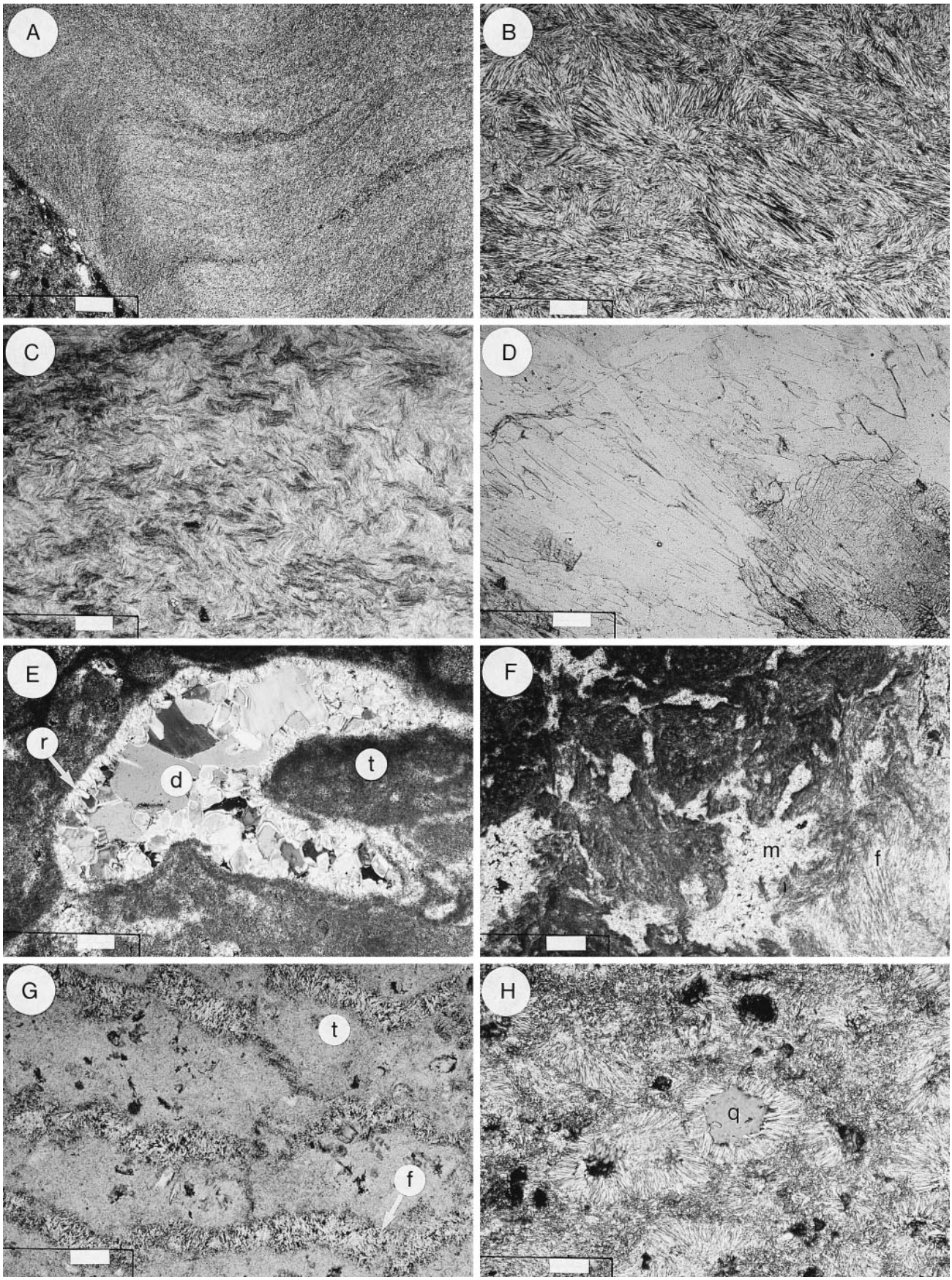

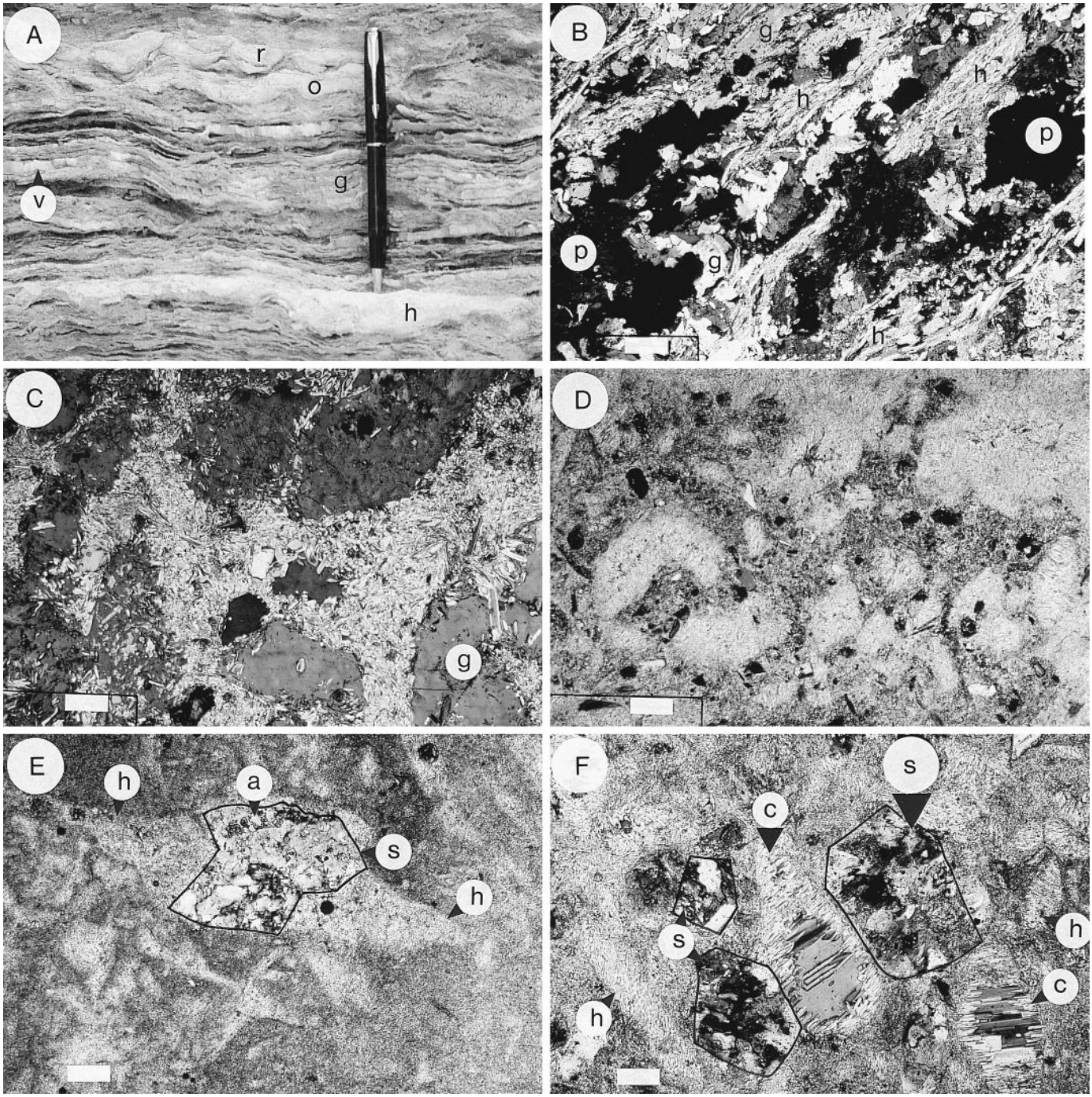


FIG. 6.—Gypsum–hydroboracite facies, and photomicrographs of fabrics. **A**) Alternation of laminated gypsum (in gray; g) and discontinuous laminae of hydroboracite (in white; h). At the top, the hydroboracite laminae show undulations (o), ripples (r), and flaser-like structures. Satin spar veins of fibrous gypsum (in white, v) are intercalated within the gypsum laminae. Pen: 15 cm. **B**) Discontinuous hydroboracite laminae of aligned-prismatic fabric (h) alternating with gypsum laminae (alabastrine secondary gypsum) (g). Abundant porosity is present (p). Crossed nicols. Bar: 0.16 mm. **C**) Fine-grained, microgranular to prismatic hydroboracite is present as a matrix of (precursor) gypsarenite crystals (g). The hydroboracite matrix partly replaced the (precursor) gypsarenite crystals. Such precursors are currently formed by a single crystal of secondary gypsum (in gray) enclosing all them. Crossed nicols. Bar: 0.08 mm. **D**) Pseudomorphs (in white) of fine-grained, microprismatic hydroboracite after interstitially grown (precursor) gypsum crystals embedded in a hydroboracitic–tuffaceous matrix. Crossed nicols. Bar: 0.16 mm. **E**) Two superimposed generations of pseudomorphs after interstitially grown (precursor) gypsum. Type I is represented by equant to tabular, deformed pseudomorphs, varying in size, composed of fine-grained hydroboracite (h). A pseudomorph of secondary gypsum (s; the boundary of this pseudomorph appears in heavy line) bearing anhydrite relics (a) represents type II; this pseudomorph crosscuts the largest hydroboracite pseudomorph of type I, which occupies the central part of the picture (probably, this pseudomorph of secondary gypsum comprises two precursor gypsarenite crystals). Crossed nicols. Bar: 0.16 mm. **F**) Two types of pseudomorphs after interstitially grown (precursor) gypsum, which are embedded in a hydroboracitic–tuffaceous matrix. Type I is formed by pseudomorphs composed of microcrystalline to prismatic hydroboracite (h) as well as a combination of prismatic hydroboracite (outer zones) and secondary gypsum (inner zones) (c). Type II is formed by secondary gypsum pseudomorphs (s; the boundaries of these pseudomorphs appear in heavy lines). Crossed nicols. Bar: 0.08 mm.

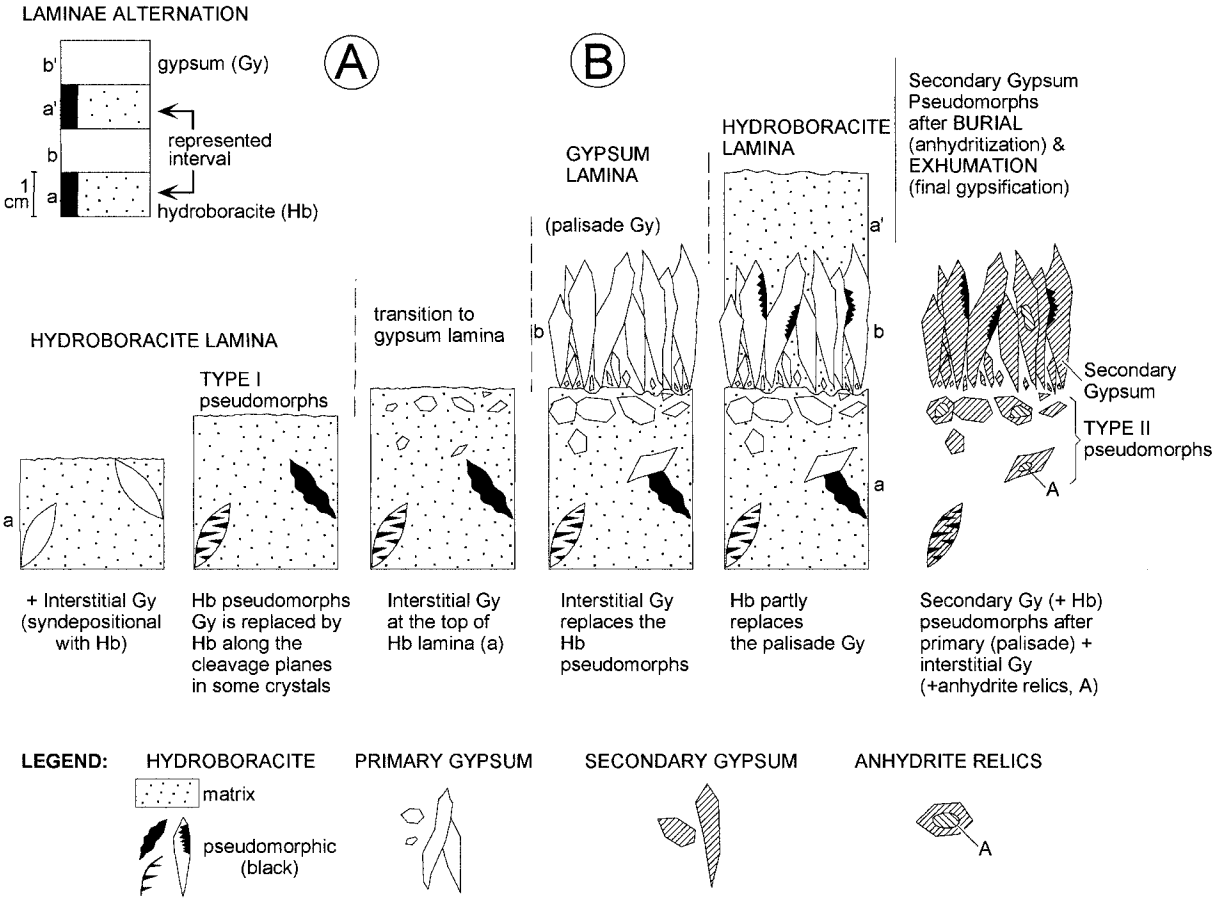


FIG. 7.—Interpretative scheme of the formation of several pseudomorphic generations in the hydroboracite laminae of the gypsum–hydroboracite alternations. The precursor crystals of all these pseudomorphs precipitated from interstitial brines under syndepositional conditions.

### *Inyoite, Colemanite, and Ulexite*

Inyoite is widely distributed in the Monte Amarillo Member either alone or accompanying other borates. The main facies are the following: crystalline–stratiform (Fig. 8A), nodules, sometimes resembling desert rosettes (Fig. 8B, C), isolated crystals and crystalline aggregates, radial or fan-shaped masses, and satin spar veins (Table 4). Crystalline stratiform inyoite can be interpreted as (mineralogically) primary owing to its significant lateral continuity to the kilometer scale. These primary precipitates seem to have occurred mainly as displacive, interstitial growths in a soft sediment under synsedimentary conditions, and there is no evidence to suggest subaqueous precipitation. In some cases, however, the petrographic observations indicate that these crystalline–stratiform facies locally replaced micronodules that were formed by a (precursor) fibrous texture. This texture can be interpreted as ulexite (Helvaci and Ortí 1998). Nodules and radial masses of inyoite can be regarded as early diagenetic growths; some of the nodules grew interstitially in the hydroboracite layers (Fig. 8C). In contrast, some inyoite nodules that replace gypsum layers could be early or late diagenetic. Crystalline aggregates of inyoite are interpreted either as early diagenetic (stratiform relation with layering) or late diagenetic (crosscutting relations).

Colemanite displays an irregular distribution, being absent in some districts of the Monte Amarillo Member. The main facies distinguished are: nodular, micronodular (Fig. 8D), radial aggregates, crystalline masses, and cementing satin spar veins (Table 4). Petrographically, cementing to replacive masses (anhedral poikilitic to blocky mosaic) of colemanite (Fig. 8E), and isolated porphyroblasts (Fig. 8F) are observed. Given the absence of pseudomorphs or relics of precursor borates in both the micronodules and the small radial aggregates, these facies can be interpreted as interstitial growths of (mineralogically) primary colemanite that precipitated under synsedimentary conditions. The displacive, cementing or replacive character of the colemanite micronodules and radial aggregates was probably controlled by the degree of lithification of the matrix. In two cases, however, these colemanite facies replaced (1) micronodules composed of a (precursor) fibrous texture that can be interpreted as ulexite (Fig. 8G, H), and (2) lenticular to euhedral crystals of (precursor) gypsum. Regarding the second case, several features indicate that this replacive colemanite predates the growth of the secondary gypsum (Table 4). Moreover, it should be emphasized that cementing to replacive colemanite masses preserved the shapes and the open fabric of the (precursor) gypsarenite crystals (Fig. 8E). These observations, together with the precise stratigraphic control of the micronodules as well as the dominant displacive character of these facies, suggest that colemanite is mainly an early diagenetic mineral that followed precipitation of the gypsarenite.

Ulexite is a scarce borate mineral in the Monte Amarillo Member, occurring as a fibrous material. In some cases the nodular facies of ulexite with a stratiform arrangement can be regarded as primary precipitates. However, the irregular distribution of this mineral, which is in many places linked to fractures, suggests that it is mainly a secondary product resulting from alteration of other borates near the surface.

## HYDROBORACITE SUBBASINS

Two main hydroboracite-bearing lithologic units can be distinguished in the Monte Amarillo hydroboracite subbasin (Section 7, Fig. 9): a hydro-

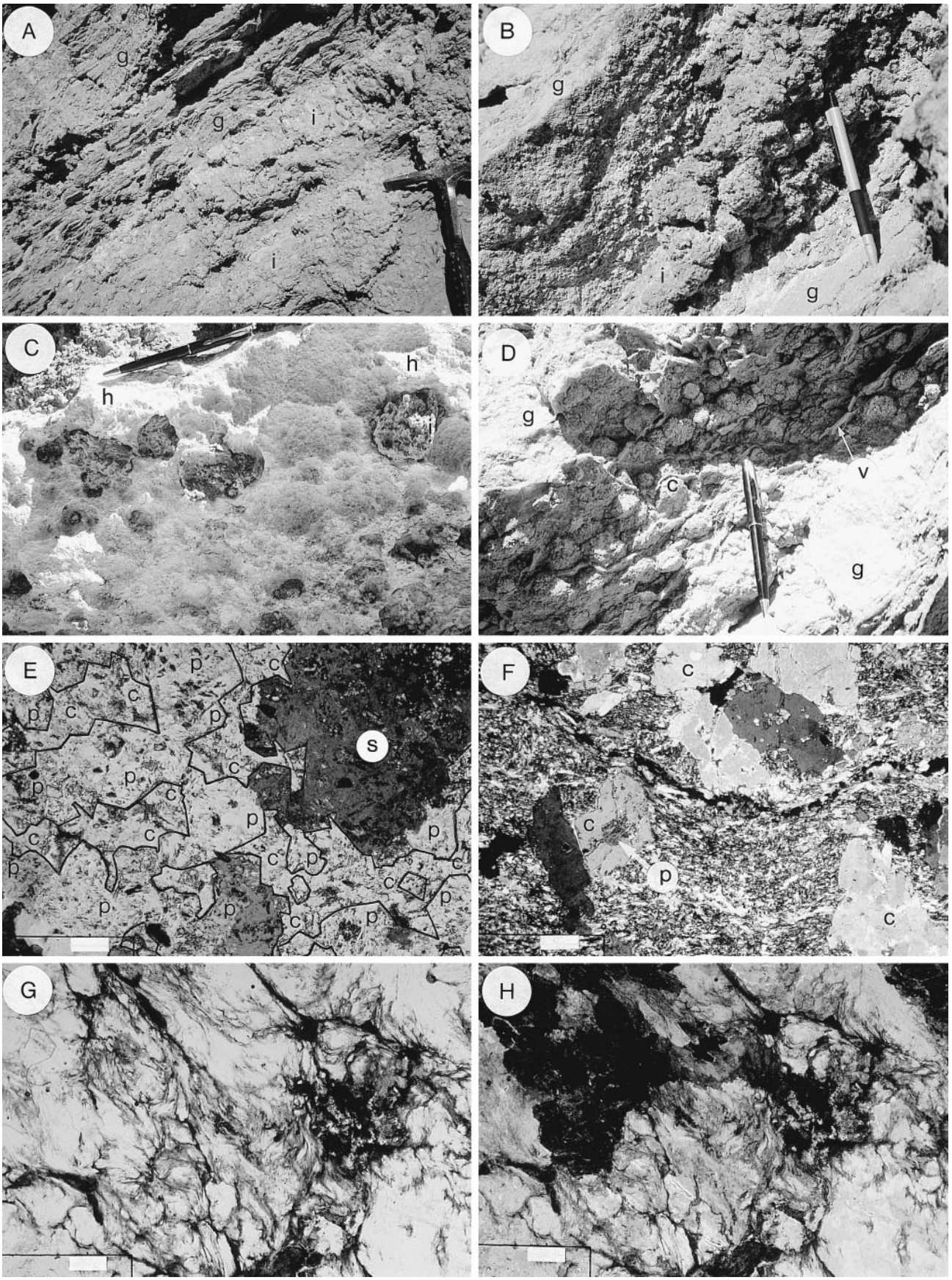

boracite unit devoid of sulfate, at the base, and a gypsum–hydroboracite unit, at the top. In the latter, gypsum and hydroboracite layers alternate; this section also shows small amounts of inyoite and minor ulexite. Toward the north, the sections of the Monte Azul mine (Section 6, Fig. 9) and the Apalacheana mine (Section 5, Fig. 9) show decreasing thicknesses of hydroboracite layers. The Monte Azul mine section has a gypsum-free hydroboracite unit. The Apalacheana mine section has a hydroboracite unit with intercalated gypsum layers. Overlying this unit is a hydroboracite-free gypsum unit 20 m thick. The proposed stratigraphic correlation between these three sections (Fig. 9) is based on the lateral continuity of the hydroboracite unit, and its lithologic and sedimentary features observed in the open-pit mines. The most significant features of this correlation are the following: (1) the hydroboracite-bearing units grade upward into hydroboracite-free (only gypsum) units; and (2) laterally, the hydroboracite-bearing units become progressively enriched with gypsum toward the north (from Section 7 to Section 5). Farther north, the section of the Ona mine (Section 4, Fig. 1A) contains gypsum layers with colemanite, inyoite, and subordinate ulexite, suggesting the disappearance of hydroboracite between this and the Apalacheana mine section. Alonso (1986) studied a section 317 m thick in the Monte Amarillo district (Fig. 10). In this section, up to six lithologic units (*a* to *f*) can be distinguished, including the hydroboracite unit (unit *d*) and the gypsum–hydroboracite unit (unit *e*) mentioned above (Section 7, Fig. 9). The distribution of evaporite minerals in these units indicates a single, thick gypsum–hydroboracite–gypsum cycle, which is slightly asymmetrical.

In the Santa Rosa hydroboracite subbasin, the Monte Amarillo Member contains alternating gypsum and hydroboracite layers, as shown in the type section (Fig. 11A). Clastic layers are irregularly intercalated within the chemical precipitates. At least two gypsum–hydroboracite cycles (I and II; Fig. 11A) can be distinguished, with individual thicknesses between 40 and 70 m. Each cycle comprises the following layers, in ascending order: (1) gypsum layers, (2) gypsum–hydroboracite alternations, and (3) hydroboracite layers. In fact, cycle II seems to be linked to a more general gypsum–hydroboracite–gypsum cycle (II–II′) that is almost symmetrical. Study of the gypsum facies in this section reveals that (1) the banded massive facies dominates the lower part of the cycles, whereas the laminated facies prevails in the upper part, and (2) the nodular facies is absent at the base of the cycles, although it accompanies the laminated facies in the upper part; these alternations of laminated and nodular gypsum facies can be interpreted as minor, shallowing-upward cycles (Fig. 11Ba). In general, the laminated gypsum prevails in the gypsum–hydroboracite alternations (Fig. 11Bb). Rhythmic alternations between laminated and intraclastic/globular facies of hydroboracite (Fig. 11Bd) also seem to represent minor, shallowing-upward cycles linked to emergent conditions. Colemanite, as micronodules and radial aggregates, is limited to the banded massive facies in all of the gypsum layers (1 in Figure 11A), and ends when the nodular gypsum facies appears. Inyoite is associated with gypsum, colemanite (Fig. 11Bc), and hydroboracite (Fig. 11Be). All these observations carried out in the two hydroboracite subbasins suggest: (1) a primary origin for the precipitation of the hydroboracite layers and the hydroboracite–gypsum alternations; (2) synsedimentary conditions for the colemanite growth; (3) absence of replacement between colemanite and inyoite; and (4) a wide range of conditions for the inyoite precipitation: inyoite aggregates forming nodules can displace also the hydroboracite laminae (Figs. 11Be, 8C).

The gypsum–hydroboracite units and cycles of the Monte Amarillo and Santa Rosa subbasins, respectively, are represented in Figure 12. The Monte Amarillo subbasin contains a single hydroboracite unit (unit *d*, Fig. 10), which grades laterally into a gypsum–hydroboracite alternation in the Apalacheana mine section. Figure 12 assumes a symmetrical arrangement toward the south (the Monte Marrón district, Section 9). Overlying this hydroboracite unit is a gypsum–hydroboracite unit (unit *e*, Fig. 10), which

TABLE 4.—*Facies and crystalline fabrics of inyoite and colemanite (Fig. 8).* **(1)** *characteristics* **(2)** *stratigraphy* **(3)** replacive/displacive origin **(4)** pseudomorphs.

**INYOITE: Crystalline-stratiform inyoite**

**(1)** Massive (up to 20 cm thick) layers composed of an interlocking crystalline mosaic (crystals are <1 cm long) of inyoite. **(2)** Intercalated between claystone, tuff, gypsum, and hydroboracite layers; it is located at the bases and at the tops of the hydroboracite beds. **(3)** Mainly displacive; this facies rarely replaces micronodules of ulexite.

**Isolated crystals and crystalline aggregates (inyoite)**

**(1)** Euhedral, macroscopic (up to few cm long) crystals embedded in claystone, gypsum, hydroboracite, and tuff layers. These crystals can occur individually or grouped into aggregates. **(2) (3)** Many aggregates are commonly arranged parallel to bedding; others cut the stratification obliquely and are late diagenetic.

**Nodular inyoite**

**(1)** Spherical to elongated shapes, formed by inyoite crystals up to few mm long (in general, <1 cm long). **(2) (3)** The nodules displace the lamination in the gypsum or hydroboracite layers; they can also be replacive.

**Radial, fan-shaped masses (inyoite)**

**(1)** Crystalline masses of up to 20 cm long, formed by medium grained inyoite crystals (crystals up to a few mm in width). **(2) (3)** These masses displace and poikilitically cement claystone and tuff layers.

**COLEMANITE: Nodular colemanite**

**(1)** Small, dirty nodules are <3 cm in diameter (micronodules); larger nodules are rarely found, always <10 cm in diameter. **(2)** They are abundant in some claystone and gypsum layers. **(3)** Micronodules can displace (most commonly), poikilitically cement, or less frequently replace the matrix; colemanite rarely replaces micronodules of precursor fibrous ulexite. **(4)** Colemanite pseudomorphs after primary gypsum are observed.

**Radial aggregates (colemanite)**

**(1)** Small (up to 3 cm in diameter) aggregates of crystals which display a radial fabric. **(2)** Same distribution as nodules. **(3)** These aggregates are replacive and displacive. **(4)** Pseudomorphs after gypsum are present.

**Crystalline-massive colemanite**

**(1) (2)** Layers up to 20 cm thick of massive crystalline colemanite are rarely intercalated between claystone and gypsum layers; these masses can display a vuggy porosity. Subordinate inyoite is present locally. **(3)** This colemanite can incorporate or replace the matrix. **(4)** Pseudomorphs after lenticular gypsum are common.

**Petrographic criteria for an early diagenetic origin of colemanite micronodules and cementing masses: (a):** Some subhedral to euhedral crystals of colemanite displace the (precursor) gypsum crystals (currently, secondary gypsum pseudomorphs after primary gypsum) (*the gypsarenite was unlithified when colemanite grew*). **(b):** Anhedral, poikilitic colemanite cements the precursor gypsum crystals (currently, pseudomorphs after secondary gypsum), which were preserved from compaction (*colemanite growth predates significant compaction of the gypsarenite*). **(c):** Anhydrite fabrics seem to replace the colemanite crystals locally (*colemanite seems to predate replacive anhydrite*). **(d):** Secondary gypsum fabrics can replace the colemanite porphyroblasts locally; satin spar gypsum veins can crosscut the colemanite crystals; when the secondary gypsum rocks have been tectonically deformed, the secondary gypsum fabric surrounds the colemanite crystals (*colemanite porphyroblasts predate the deformation of the secondary gypsum rock; probably, they also predate the anhydrite formation*).

←

FIG. 8.—Facies of inyoite and colemanite, and photomicrographs of colemanite fabrics. **A**) Inyoite layers (i) formed by vertically elongated, crystalline-stratiform facies and small nodules. These layers are overlain by laminated gypsum (g). Gray material is clay. Hammer for scale. **B**) Nodules and desert-rosette facies of crystalline inyoite (i) forming a horizon in the central part of the picture; this horizon is intercalated between two gypsum layers (g). Pencil is 14 cm long. **C**) Nodules of inyoite (i; in gray) and their casts, at the top of a hydroboracite bed (h; in white). Pen is 15 cm long. **D**) Small nodules of colemanite (c) in association with clay; satin spar veins (v) of gypsum surround some colemanite nodules. This association is intercalated between two gypsum layers (g). **E**) Pseudomorphs (p) of secondary gypsum after (precursor) euhedral gypsarenite crystals. These pseudomorphs are cemented by anhedral, poikilitic masses of colemanite (c; the contact between the two minerals appears in heavy line). Note the open fabric of the pseudomorphs, suggesting that colemanite cementation preceded any significant compaction of the gypsarenite. Most impurities within the pseudomorphs are anhydrite relics. All the transparent pseudomorphs are currently composed of one crystal of secondary gypsum. Another crystal of secondary gypsum (s) is seen in optical extinction. Crossed nicols. Bar: 0.16 mm. **F**) View of a tectonically deformed fabric of secondary gypsum. Isolated and grouped subhedral porphyroblasts of colemanite (c) are embedded in an alabastrine secondary gypsum matrix. This matrix surrounds the porphyroblasts and partly replaces them, thus suggesting that the porphyroblasts predate the deformation of the secondary gypsum fabric. A secondary gypsum pseudomorph after (precursor) gypsarenite (p; in gray) is preserved in one of the colemanite porphyroblasts. Crossed nicols. Bar: 32 mm. **G, H**) Partial view of a colemanite micronodule. In normal light (G), a flowage fabric of a (precursor) fibrous mineral (presumably micronodular ulexite) can be distinguished. In crossed nicols (H), large, anhedral crystals of colemanite replace the micronodular fabric irregularly. Bar: 0.32 mm.

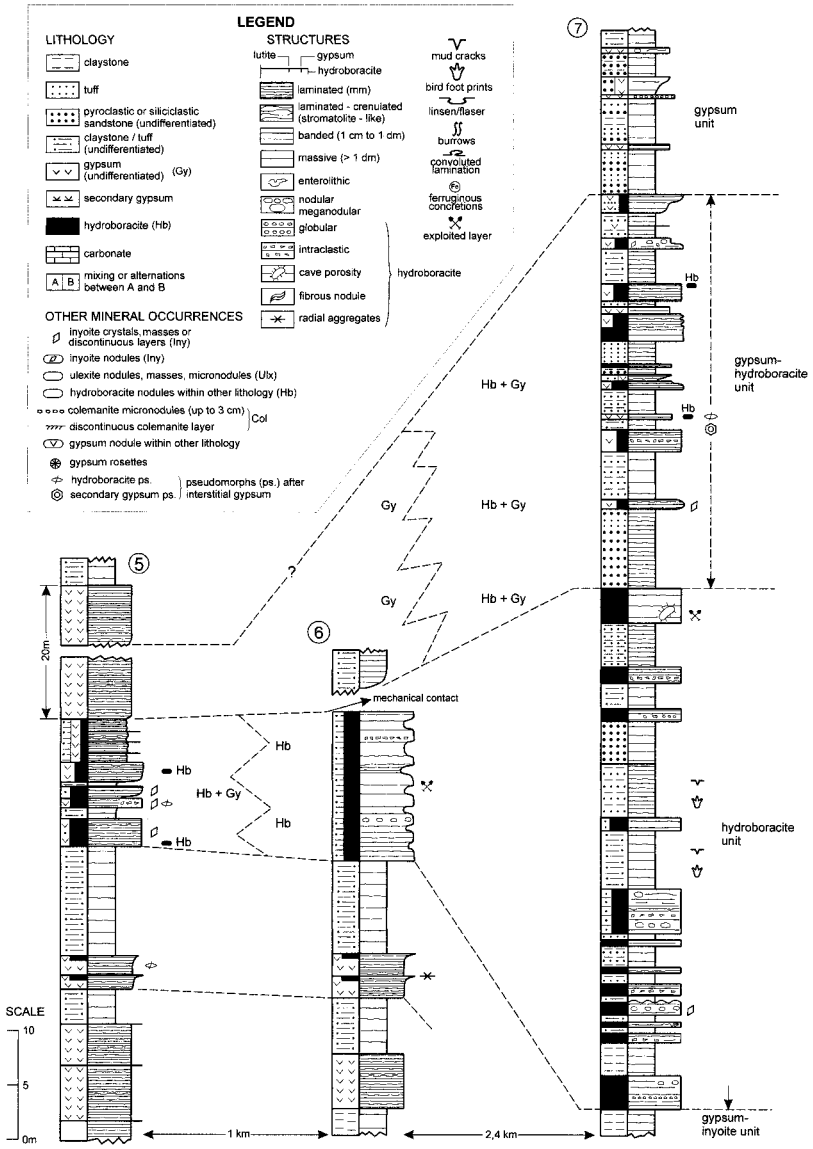


FIG. 9.—Partial (limited to the borate-bearing parts) stratigraphic sections of the Monte Amarillo Member in the Apalacheana mine (5), the Monte Azul mine (6), and the Monte Amarillo borate district (7) (see location in Fig. 1A). The lithologic units and the proposed correlation are indicated. Col, colemanite; Iny, inyoite; Ulx, ulexite; Hb, hydroboracite.

grades laterally into hydroboracite-free gypsum layers. The chemical zonation observed in this subbasin suggests the existence of the following depositional belts: (1) a gypsiferous belt in the outermost part, which contains some inyoite toward the inner zone (the lake center); (2) an intermediate belt, in which a gypsum–hydroboracite alternation bearing some inyoite is recorded; and (3) a central body, with prevalent hydroboracite, and minor inyoite. The Santa Rosa subbasin displays a facies arrangement characterized by several gypsum–hydroboracite cycles (Fig. 11A) that cannot be correlated with the units of the Monte Amarillo subbasin. Presumably, local conditions of subsidence, structure, and depositional controls resulted in differentiated models of chemical sedimentation for the two subbasins. The interpreted depositional belts are similar to those in the Monte Amarillo subbasin, although here, for each cycle some colemanite can be present in association with gypsum. The zone corresponding to the Ona mine (Section 4) behaves as a shoal linking the two subbasins. All the hydroboracite layers thin out toward this shoal, and only colemanite, ulexite, and inyoite are recorded as the lateral equivalent of hydroboracite. In the opposite directions the two subbasins lose the hydroboracite, and only colemanite, inyoite, and ulexite are found.

## DISCUSSION: SEDIMENTOLOGIC AND DIAGENETIC CONDITIONS OF THE SULFATE–BORATE ASSOCIATION

### *Sedimentary Stages and Origin of the Hydroboracite*

The aforementioned chemical zonation corresponds to the following lateral succession of precipitates, from the margin to the center of the subbasins: calcium sulfate → calcium borate → calcium/magnesium borate. This zonation together with the presence of the gypsum–hydroboracite cycles (Fig. 11A) allows us to envisage a lacustrine evolution (Fig. 13A) from the initial dry mud flat (stage 1) to the lake oversaturated in hydroboracite (stage 5). Figure 13B illustrates this evolution as a vertical sequence in which colemanite is linked to gypsum, whereas inyoite can accompany precipitation of both gypsum/anhydrite, and hydroboracite. Accumulation of gypsum-free hydroboracite requires sulfate depletion in the precipitating brine, and it seems likely that the episodes of anhydrite formation favored this depletion, although probably stage 4 was not strictly necessary for hydroboracite precipitation. In some cases, pure hydroboracite is achieved immediately after the calcium sulfate stage (unit *d*, Fig. 10), although commonly such precipitation is preceded or followed by a

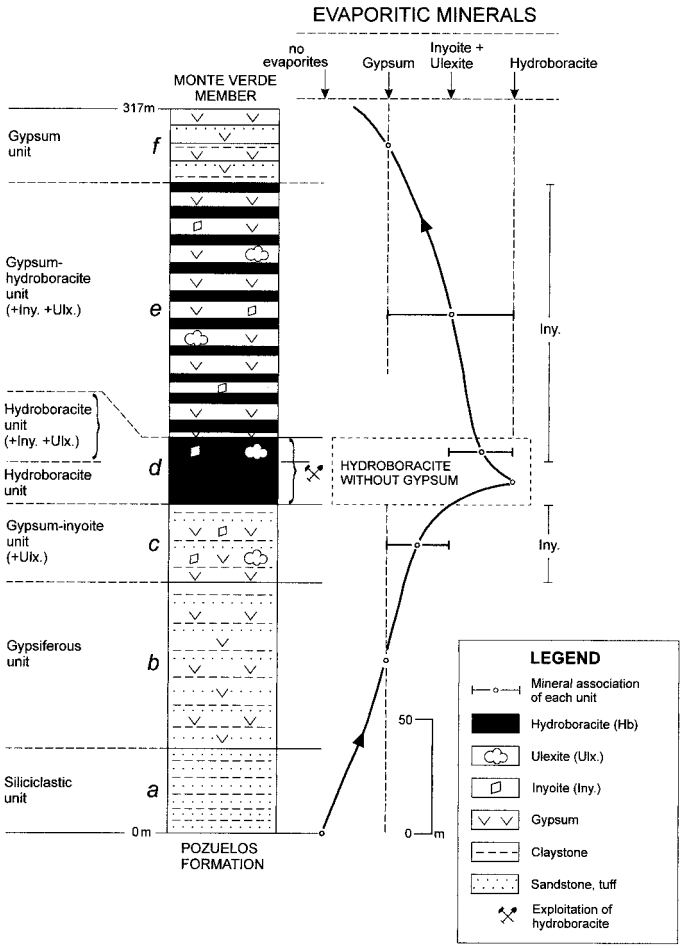


FIG. 10.—Type section of the Monte Amarillo Member (adapted from Alonso 1986). On the right side, the line shows the mineralogical evolution of the sequence: the lower part (*a* to *d* units) evolves from gypsum, and gypsum + inyoite, to hydroboracite, whereas the upper part (*e* and *f* units) is characterized by a thick unit (*e*) of hydroboracite + gypsum, evolving to gypsum.

mixed gypsum–hydroboracite alternation (layers 2 in Fig. 11A, and unit *e* in Fig. 10, respectively), involving stages 3 to 5. Thus, precipitation of calcium sulfate in the Sijes Formation clearly predates that of borate. Similar observations have been made by Alonso (1986) in several modern salars in Puna region.

The genesis of the Mg-bearing borates is a complex subject. In the first place, hydroboracite in the Holocene and modern saline lakes is very scarce, being limited mostly to efflorescent crusts in which hydroboracite is associated with numerous evaporitic minerals. In the second place, the Mg-bearing borates occur mainly as accessory minerals in several Neogene lacustrine deposits of both the colemanite–ulexite type and the borax type (Crowley 1996). The investigations carried out on these deposits usually assign the Mg-bearing minerals either (1) to the diagenetic reaction of ulexite, probertite, colemanite, or borax with the clay minerals, or (2) to the alteration of borate minerals under the action of groundwaters rich in magnesium. As far as hydroboracite is concerned, the stratigraphic and textural studies made in some deposits seem to be consistent with a diagenetic or an alteration origin from other borates, mainly from colemanite (Minette and Wilbur 1973; Barker 1980; Countryman 1977). Nevertheless, Crowley (1996) proposed an alternative explanation for the Mg-bearing borates based on the primary origin. According to this author, these borates would have been produced by chemical fractionation of the brines under progressive evaporation. During the evaporative process, the calcium is first fractionated by means of the precipitation of both calcium carbonate, and calcium and calcium/sodium borates (inyoite, colemanite, ulexite). Subsequently, magnesium or calcium/magnesium borates are formed, these precipitates being the end products of the brine concentration. The path diagram used by Crowley (1996) includes hydroboracite as the final product of the following evolutionary line: gypsum $\rightarrow$ ulexite $\rightarrow$ hydroboracite $\rightarrow$ (Na, $SO_4$, Cl) end brine, which can be expected from waters with the appropriate Ca/Mg molar ratio.

Our sedimentologic observations made on the hydroboracite deposits of the Sijes Formation lends support to Crowley's interpretation. This hydroboracite was probably formed in relatively shallow lakes (up to a few meters deep?), which were affected by recurrent fluctuations of the water level. The observations by Sun and Li (1993), made in numerous recent saline lakes in the Tibet plateau, indicate that (1) Mg-borates are mainly related to brines of the sulfate type, and (2) some relatively deep, perennial lakes are currently precipitating Mg-borates under low-temperature conditions. The sulfate–borate association of the Sijes Formation seems to represent a minor variation of the sequence—involving hydroboracite—discussed by Crowley (1996), in which relatively important deposits of colemanite–ulexite should precede precipitation of the Mg-borates. In contrast, the important gypsum/anhydrite precipitation in the Sijes Formation appears to have caused a decrease in calcium content in the brine, thus limiting precipitation of calcium borates (inyoite, colemanite). Furthermore, this limited precipitation of borates during the first stage of brine evolution has favored extensive precipitation of a Mg-bearing borate accompanied by minor inyoite.

Rusansky (1985) assigned the origin of the hydroboracite of the Santa Rosa district to dehydration of inderborite to hydroboracite, despite finding no pseudomorphs or relics of the more hydrated phase (inderborite). Rusansky's conclusion was based largely on the interpretation of the microscopic textures of hydroboracite (''fluidal textures'') as a product of intense recrystallization. In contrast, Alonso (1986) and Aristarain (1991) considered a primary origin of the hydroboracite in the Sijes Formation on the basis of mapping, stratigraphy, facies, and mineralogy. From the petrographic point of view, however, the conclusion that hydroboracite is a primary mineral requires some explanation. Although the fibrous and prismatic fabrics of hydroboracite suggest a primary origin, in some cases the textural relations also indicate that this mineral grew replacively. Thus, when hydroboracite is associated with tuff, the crystal fragments (quartz, feldspar) are largely replaced by this borate. Moreover, in the hydroboracite laminae of the gypsum–hydroboracite alternations, (1) the hydroboracite pseudomorphs indicate that this mineral replaced the precursor gypsum to some extent, and (2) the interstitially grown gypsum precursors of many secondary gypsum pseudomorphs precipitated under syndepositional conditions, replacing both the hydroboracite matrix and the preexisting hydroboracite pseudomorphs. All these pseudomorphs are commonly distributed in the gypsum–hydroboracite units of the two subbasins studied (Fig. 9; layers 2 in Figure 11A). These features suggest that during precipitation of one mineral forming a discrete lamina, e.g., gypsum, the underlying lamina of the other mineral, i.e., hydroboracite, was displaced and partly replaced by gypsum crystals growing from interstitial solutions (Fig. 7).

### *Significance of the Colemanite–Inyoite Occurrences*

In general, the mineral zonation displayed by many Neogene borate bodies in the world, which is characterized by abundant sodium borates in the inner parts and minor calcium borates in the outer parts, has been interpreted in the literature as a primary facies arrangement (Inan et al. 1973; Bowser and Dickson 1966; Kistler and Helvaci 1994). In other cases, however, these deposits have been attributed to alteration of borate minerals by groundwater action (reaction diagenesis; Smith 1985). The latter interpretation is made (1) when colemanite is prevalent toward the outer parts of the deposits, and (2) when variable amounts of accessory Mg-bearing

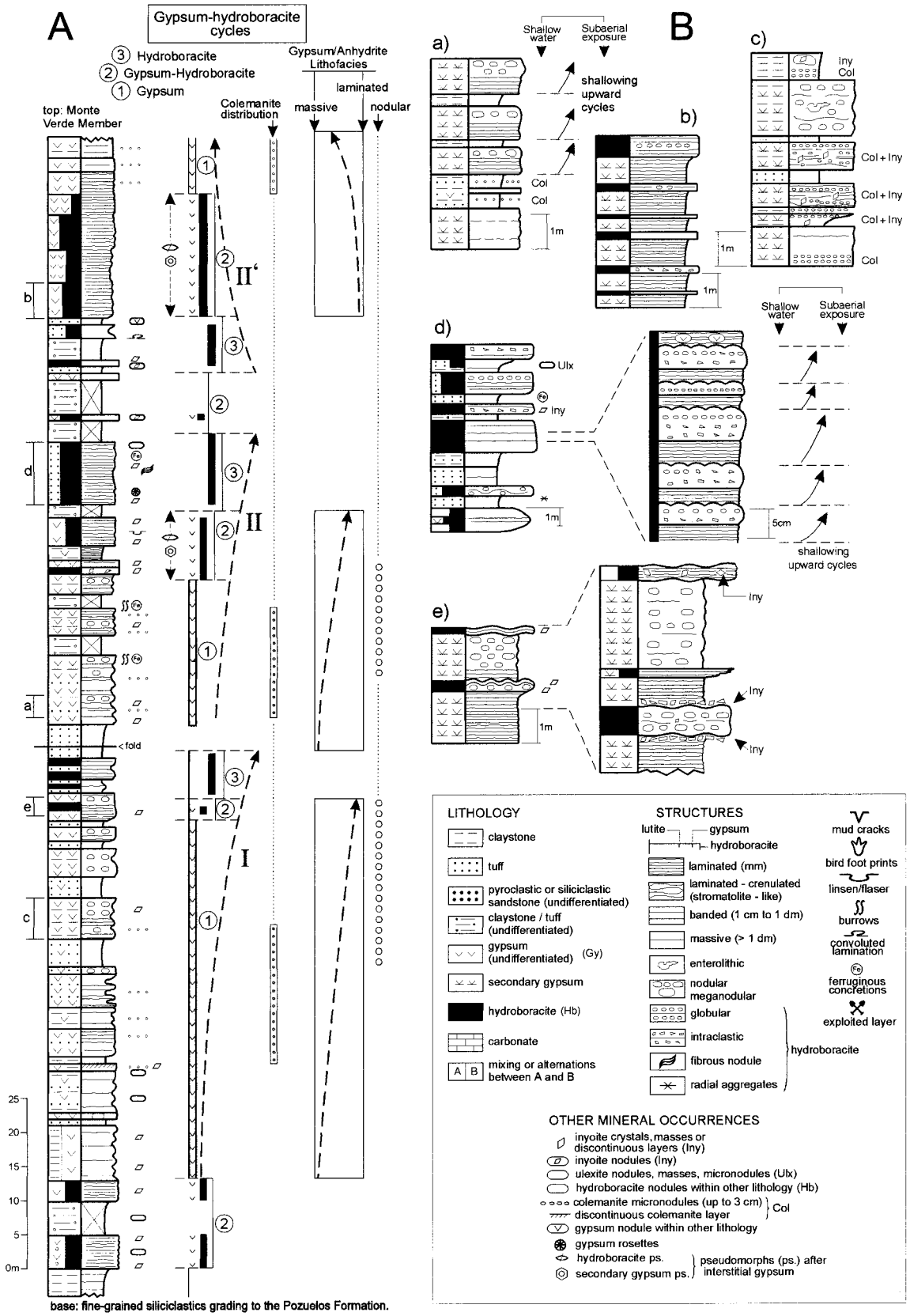


FIG. 11.—**A**) Stratigraphic section of the Monte Amarillo Member in the Santa Rosa borate district (Section 3, see location in Fig. 1A). On the left, the lithologic log is shown; in the middle, the gypsum–hydroboracite depositional cycles are indicated; on the right, the colemanite distribution in these cycles, and the main characteristics of the associated calcium sulfate facies, are shown. **B**) Enlarged parts (a to e) of the section in A showing the most outstanding facies and minor cycles.

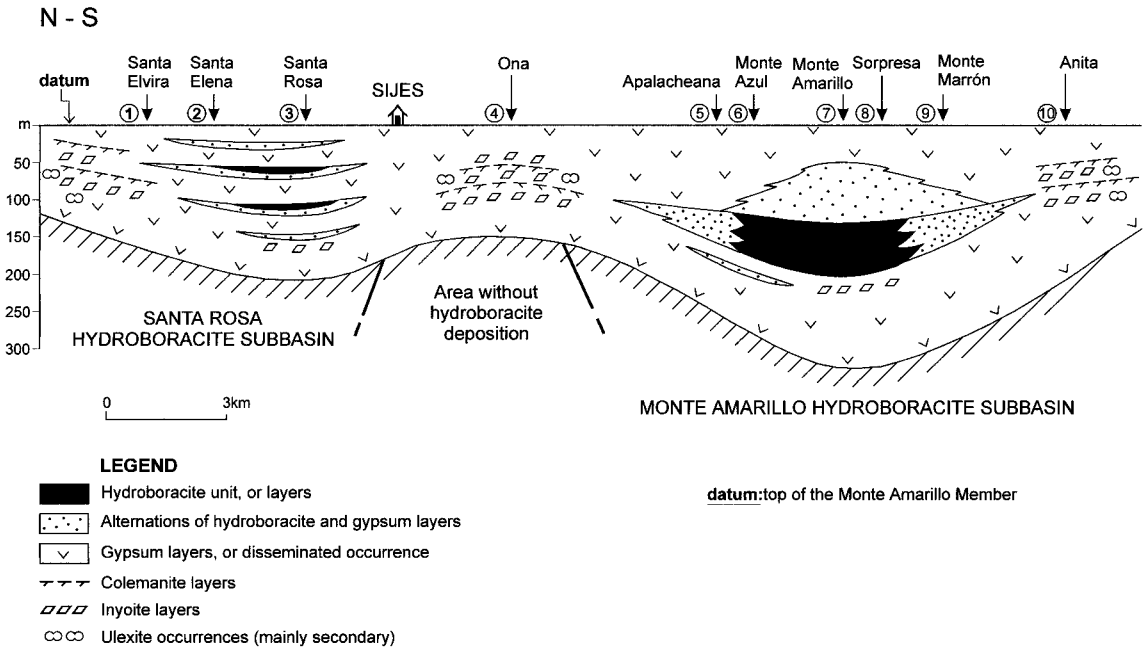


FIG. 12.—Scheme of the borate facies distribution in the Santa Rosa and the Monte Amarillo hydroboracite subbasins. The siliciclastic (mainly lutites) and tuffaceous host sediment of sulfates (gypsum) and borates is omitted. Numbered borate districts are as in Figure 1A.

borates are present. In line with this interpretation, the relative importance of colemanite, inyoite, and ulexite in the marginal zones of the two subbasins of the Monte Amarillo Member (Fig. 12) could also be regarded as the leaching products of the hydroboracite layers. Nevertheless, we propose that the mineral zonation found in this member is primary—Mg-bearing borates, instead of sodium borates, occupying the central part of the basin—and reflects the existence of a lateral gradient of the ionic concentration. Owing to this gradient, a progressive change exists from colemanite–inyoite, in marginal positions, to hydroboracite, in central positions. This interpretation is based on (1) the field observation of this mineral gradation in the absence of mineralogic replacement between the various borate minerals, and (2) the petrographic observations made in the Santa Rosa district (Fig. 11), which indicate that colemanite followed precipitation of gypsum and predated growth of anhydrite (Table 4). Coprecipitation of calcium borates and calcium sulfates is possible given that the stability ranges of colemanite, inyoite, ulexite, and gypsum overlap to a considerable degree (Crowley 1996).

The ubiquitous presence of colemanite in the Neogene borate deposits, together with the absence of this mineral in the Holocene deposits, has commonly been assigned to burial (thermal) diagenesis (Smith and Medrano 1996). This interpretation suggests that the Neogene deposits would have undergone a general inyoite (meyerhofferite)-to-colemanite transformation during burial. Nevertheless, from stratigraphic data in Alonso (1986) and Vandervoort (1993) it can be estimated that the most probable burial of the Monte Amarillo Member in the centers of the hydroboracite subbasins was about 1500 m and 1200 m in the Monte Amarillo and the Santa Rosa subbasins, respectively. The fact that inyoite is present in the thick, deeply buried Monte Amarillo subbasin (Fig. 10), whereas colemanite is present only in the thinner, less deeply buried Santa Rosa subbasin (Fig. 11A), suggests that this mineral distribution bears no relation to burial diagenesis. Probably, this distribution was controlled by depositional and/or early diagenetic factors. In contrast, the burial depth affecting the two subbasins was sufficiently large for a complete conversion of gypsum into anhydrite (Murray 1964). Thus, in the Sijes Formation we found no evidence of significant transformations between the various borate phases that could be attributed to deep burial diagenesis.

### *Provenance of the Solutes*

Fluids from hydrothermal volcanogenic systems and, to a lesser extent, weathering of Neogene volcanic rocks were considered by Alonso and Viramonte (1990, 1993) to be the main sources of the Puna solutes and of the precipitation of borates and other associated evaporites. Recently, Kaseman et al. (1998a) and Kaseman et al. (1998b) have also considered the basement rocks of the Puna plateau as a potential source of the boron supply to the Neogene borate deposits.

In the Puna plateau, many springs linked to geothermal fields have been active until very recently, or are still active. In the latter springs, the thermal waters are often connected to fractures and sites of Quaternary volcanic activity. These fluids have significant contents of volcanogenic elements such as S, B, Li, and As (Alonso 1991). Boron content can vary largely between less than 40 ppm in the Tocomar geothermal field and up to 500 ppm in the Antuco geothermal field, where a reservoir temperature of 160°C is recorded (Ferretti and Alonso 1993). Carbonate and sulfate minerals, as well as borate minerals (ulexite, borax, pinnoite, inderite) and iron and manganese oxides are common precipitates associated with all these thermal springs. Vestiges that there was similar hydrothermal activity during the Neogene in the Puna region are abundant. For instance, the Sijes Formation contains numerous travertinic (carbonate) structures linked to thermal springs that were coeval with the borate sedimentation (Alonso 1991).

Kaseman et al. (1998b) have provided data on the boron-isotope composition of the most important Neogene borate deposits (Sijes, Tincalayu, and Loma Blanca) in the Puna plateau. According to these authors, the borate minerals in each depositional unit show a sequence of decreasing $\delta^{11}B$ values from the Na-borates to the Ca-borates, which is related to the coordination of the borate minerals (Oi et al. 1989) and the precipitation of the mineral sequence at variable pH values (Palmer and Helvaci 1995). In the Sijes Sierra borate deposits of the Pastos Grandes Neogene basin, the $\delta^{11}B$ values are: $-16.8$ to $-17.2$‰ for hydroboracite, $-22.4$‰ for ulexite, and $-28.5$ to $-29.6$‰ for inyoite. These values can be compared with those of the solutions issuing from the currently active hydrothermal springs in the Puna region, in particular the Antuco spring, where the bor-

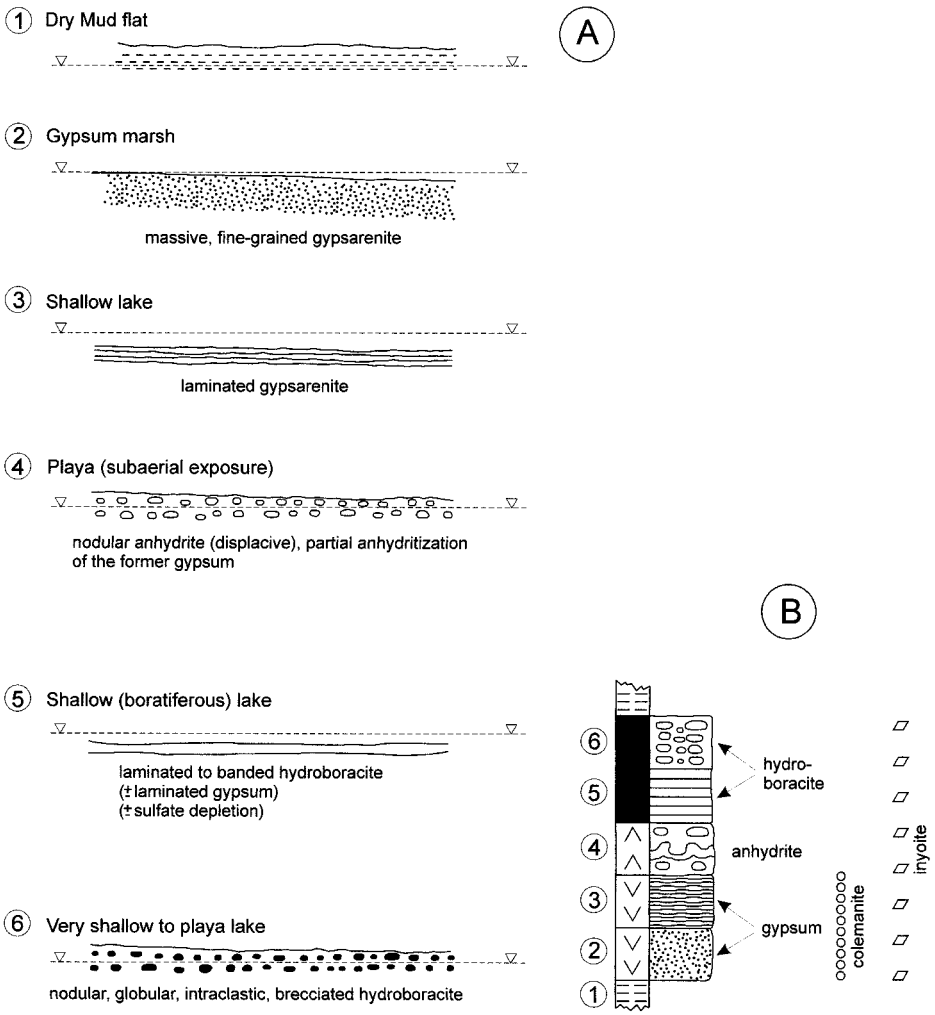


FIG. 13.—**A**) Sedimentary stages in the sulfate–borate association of the Monte Amarillo Member as interpreted from Figure 11A. **B**) Theoretical sequence obtained from the stages in part A. Note the different distribution of colemanite and inyoite in the sequence. Scheme without scale.

atiferous brine has a $\delta^{11}B$ value of $-12.5‰$ at a pH of 7.9, and the presently forming ulexite deposit has a $\delta^{11}B$ value of $-22.4‰$. Thus, on the basis of the similarity of the $\delta^{11}B$ values found in the mineral sequences from the Sijes deposits and the precipitates of the Antuco spring, Kasemann et al. (1998b) (1) deduced that the composition of the boratiferous solutions feeding the Neogene Sijes lakes was similar to those of the Antuco spring, and (2) calculated a $\delta^{11}B$ value of $-12.0‰$ for the boratiferous parent brines of the Sijes deposits. All of this suggests that the boron supply to the Neogene lacustrine systems was largely linked to the hydrothermal activity, regardless of the ultimate lithologic source (basement rocks, Tertiary volcanics) of borates. Nevertheless, given the important volcanism recorded in the Puna plateau during Neogene times, it seems likely that both the boron supply and the overall ionic composition of the lacustrine solutions were related, to some extent, to the regional magmatic and extrusive activity.

Mg-bearing borates (hydroboracite) and Ca borates (inyoite, colemanite) dominate the various boratiferous members of the Neogene Sijes Formation in the Pastos Grandes depression. Sodium appears to be a minor component of the initial solution, as demonstrated by both the small relevance of ulexite as a primary precipitate and the lack of other Na-bearing salts (glauberite, thenardite, halite). The prevalence of magnesium over other cations in the initial solutions is problematic. One explanation is that some magnesium-rich volcanic phases existed in the region during the sedimentation of the Sijes Formation. Alonso (1986) found evidence of extinct geyser and thermal-spring activity in a Quaternary deposit of the Quebrada Sococastro, close to the Pastos Grandes depression to the north. In the evaporitic precipitates of this deposit, a boron/magnesium character was confirmed by the presence of pinnoite and inderite, as well as by a high content of magnesium (up to 18.72%). According to this, a local, coeval magnesium supply of volcanogenic origin to the Neogene Sijes lakes could be regarded as a source of magnesium to be added to other possible sources such as cation exchange with clay minerals and leaching of the country rocks.

## CONCLUSIONS

(1) In the Monte Amarillo Member, hydroboracite layers accumulated in the centers of two shallow lacustrine subbasins and gypsum along the margins, the intermediate zones being characterized by an alternation of gypsum and hydroboracite. Calcium borates precipitated mainly along the margins, where they represent facies gradation from hydroboracite. This mineral zonation involving sulfates and borates is depositional.

(2) In the vertical sequence of the centers, the calcium sulfate (as gypsarenite and syndepositional anhydrite), which was accompanied by subordinate calcium borates (colemanite and/or inyoite), precipitated first. Subsequently, hydroboracite precipitated in association with subordinate inyoite. The high sulfate content in the initial solution could have controlled the progressive impoverishment of Ca. The purest hydroboracite precipitate was achieved only after significant sulfate depletion in the brine.

(3) Hydroboracite is mainly a primary precipitate, and no precursor bo-

rate was identified. Nevertheless, some gypsum was replaced by hydroboracite in the gypsum–hydroboracite alternations under synsedimentary conditions. This replacement clearly predated the generalized gypsum-to-anhydrite transformation during moderate burial.

(4) Colemanite and some inyoite precipitated interstitially as (mineralogically) primary phases under synsedimentary conditions, and no mutual replacement between them was observed. In general, these minerals displaced or cemented the sedimentary matrix, but they also replaced the gypsarenite locally. There is no evidence to suggest that colemanite had a precursor borate, except rare ulexite micronodules. Evidence of transformations of the borate minerals during deep burial diagenesis was not found.

## ACKNOWLEDGMENTS

The authors wish to thank to BORAX ARGENTINA S.A. (Campo Quijano, Salta, Argentina) and the manager and geologist for field assistance and facilities in the Sijes locality. We also thank Dr. C. Helvaci and Dr. L. Rosell for their comments on an earlier draft of this paper, J. Illa (Universitat de Barcelona) for preparing the petrographic collection, and the Serveis de Dibuix i Disseny Gràfic of the Universitat de Barcelona for drafting assistance. This research was financed by the Spanish projects PB94-0882 and PB97-0905 (Dirección General de Investigación Científica y Técnica) and forms part of the program on Andean borates carried out by R. N. A. for the Consejo Nacional de Investigación Científica y Técnica (CONICET), Argentina, and the Consejo de Investigación de la Universidad Nacional de Salta (CIUNSA, projects 509 and 551). F.O. benefited from a grant from the Spanish Ministerio de Educación y Cultura, for a three-month stay in the Universidad Nacional de Salta (Argentina) in 1998. The authors acknowledge Dr. B.C. Schreiber, Dr. S. Hovorka, and Dr. M. El Tabakh for very constructive reviews.

## REFERENCES

Allmendinger, R.W., 1986, Kinematic and tectonic history of the southern margin of the Puna plateau, northwest Argentina: Geological Society of America, Bulletin, v. 97, p. 1070–1082.

Alonso, R.N., 1986, Ocurrencia, posición estratigráfica y génesis de los depósitos de boratos de la Puna Argentina [doctoral thesis]: Universidad Nacional de Salta, Argentina, 196 p.

Alonso, R.N., 1991, Evaporitas neógenas de los Andes Centrales, *in* Pueyo, J.J., ed., Génesis de Formaciones Evaporíticas. Modelos Andinos e Ibéricos: Estudi General 2, Universitat de Barcelona, p. 267–329.

Alonso, R.N., 1992, Estratigrafía del Cenozoico de la cuenca de Pastos Grandes (Puna salteña) con énfasis en la Formación Sijes, y sus boratos: Asociación Geológica Argentina, Revista, v. 47, p. 189–199.

Alonso, R.N., and Viramonte, J.G., 1990, Borate deposits in the Andes, *in* Fontboté, L., Amstutz, G.C., Cardozo, M., Cedillo, E., and Frutos, J., eds., Stratabound Ore Deposits in the Andes: Heidelberg, Springer-Verlag, p. 721–732.

Alonso, R.N., and Viramonte, J.G., 1993, La cuestión genética de los boratos de la Puna: XII Congreso Geológico Argentino / II Congreso Exploración Hidrocarburos, Mendoza, Actas, v. 5, p. 187–194.

Alonso, R.N., Jordan, T.E., Tabbutt, K.T., and Vandervoort, D.S., 1991, Giant evaporite belts of the Neogene Central Andes: Geology, v. 19, p. 401–404.

Aristarain, L.F., 1991, Hidroboracita, $CaO{\cdot}MgO{\cdot}B_2O_3{\cdot}6H_2O$, del distrito de Sijes, Salta, Argentina: Museo Argentino Ciencias Naturales Bernardino Rivadavia, Revista Geología, v. 10 (1), p. 3–24.

Aristarain, L.F., and Hurlbut, C., 1972, Boron, Minerals and Deposits: Tucson, Arizona, The Mineralogical Record, v. 3, p. 213–220.

Barker, C.E., 1980, The Terry borate deposits, Amargosa Valley, Inyo Country, California: California Geology, v. 33, p. 181–187.

Bowser, C.J., and Dickson, F.W., 1966, Chemical zonation of the borates of Kramer, California, *in* Rau, J.L., ed., 2nd Symposium on Salt, vol. 1: Cleveland, Northern Ohio Geological Society, p. 122–132.

Catalano, L.R., 1926, Geología de los yacimientos de boratos y materiales de las cuencas. Salar de Cauchari. Puna de Atacama: Buenos Aires, Dirección General de Minas, Geología e Hidrogeología, Publicación 23, p. 1–110.

Countryman, R.L., 1977, Hydroboracite from Amargosa Desert, Eastern California: Tucson, Arizona, The Mineralogical Record, v. 8, p. 503–504.

Crowley, J.K., 1996, Mg- and K-bearing borates and associated evaporites at Eagle Borax Spring, Death Valley, California: A spectroscopic exploration: Economic Geology, v. 91, p. 622–635.

El Tabakh, M., Schreiber, B.C., and Warren, J.K., 1998, Origin of fibrous gypsum in the Newark Rift Basin, Eastern North America: Journal of Sedimentary Research, v. 68, p. 88–99.

Ferretti, J.I., and Alonso, R.N., 1993, Geoquímica del campo geotérmico Tocomar (Salta): XII Congreso Geológico Argentino, II Congreso de Exploración de Hidrocarburos, Mendoza, Actas, v. 5, p. 311–316.

Helvaci, C., 1995, Stratigraphy, mineralogy and genesis of the Bigadiç borate deposits, western Turkey: Economic Geology, v. 90, p. 1237–1260.

Helvaci, C., and Ortí, F., 1998, Sedimentology and diagenesis of Miocene colemanite–ulexite deposits (western Anatolia, Turkey): Journal of Sedimentary Research, v. 68, p. 1021–1033.

Igarzábal, A., 1979, Los rasgos geomorfológicos y su relación con el origen del Salar Pastos Grandes, departamento de los Andes, Provincia de Salta: 7° Congreso Geológico Argentino, Actas I, p. 199–209.

Igarzábal, A., 1991, Evaporitas cuaternarias de la Puna Argentina, *in* Pueyo, J.J., ed., Génesis de Formaciones Evaporíticas. Modelos Andinos e Ibéricos: Estudi General 2, Universitat de Barcelona, p. 333–374.

Inan, K., Dunham, A.C., and Esson, J., 1973, Mineralogy, chemistry and origin of Kirka borate deposits, Eskisehir Province, Turkey: Institution of Mining and Metallurgy, Transactions, Sect. B, v. 82, p. 114–123.

Isacks, B.L., 1988, Uplift of the central Andean plateau and bending of the Bolivia orocline: Journal of Geophysical Research, v. 93, p. 3211–3231.

Jordan, T.E., and Alonso, R.N., 1987, Cenozoic stratigraphy and basin tectonics of the Andes Mountains, 20°–28° south latitude: American Association of Petroleum Geologists, Bulletin, v. 71, p. 49–64.

Jordan, T.E., Isacks, B.L., Allmendinger, R.W., Brewer, J.A., Ramos, V.A., and Ando, C.J., 1983, Andean tectonics related to geometry of the subducted Nazca plate: Geological Society of America, Bulletin, v. 94, p. 341–361.

Kasemann, S., Franz, G., Erzinger, J., Viramonte, J.G., Meixner, A., and Tonn, S., 1998a, Geochemistry and isotope geochemistry of boron. An overview from Precambrian to Recent in the central Andes, NW Argentina: 16th Coloquio Latinoamericano de Ciencias, Terra Nostra, v. 98 (5), p. 78–79.

Kasemann, S., Franz, G., Erzinger, J., Viramonte, J.G., and Alonso, R.N, 1998b, Boron isotopic composition of Tertiary borate deposits in the Puna plateau of the central Andes, NW Argentina: X Congreso Latinoamericano de Geología y VI Congreso Nacional de Geología Económica, Actas, v. 3, p. 56.

Kistler, R.B., and Helvaci, C., 1994, Boron and borates, *in* Carr, D.D., ed., Industrial Minerals and Rocks, 6th Edition: Society for Mining, Metallurgy, and Exploration, p. 171–186.

Minette, J.W., and Wilbur, D.P., 1973, Hydroboracite from the Thompson mine, Death Valley: Tucson, Arizona, The Mineralogical Record, v. 4, p. 21–23.

Murray, R.C., 1964, Origin and diagenesis of gypsum and anhydrite: Journal of Sedimentary Petrology, v. 34, p. 512–523.

Oi, T., Nomura, M., Musashi, M., Ossaka, T., Okamoto, M., and Kakihana, H., 1989, Boron isotopic compositions of some boron minerals: Geochimica et Cosmochimica Acta, v. 53, p. 3189–3195.

Ortí, F., 1977, Aproximación al estudio petrográfico de las microestructuras de las rocas de yeso secundario y a su orígen: Instituto de Investigaciones Geológicas, Diputación Provincial de Barcelona, v. 32, p. 87–152.

Ortí, F., 1997, Evaporite sedimentation in the South Pyrenean Foredeeps and the Ebro basin during the Tertiary: a general view, *in* Busson, G., and Schreiber, B.C., eds., Sedimentary Deposition in Rift and Foreland Basins in France and Spain: New York, Columbia University Press, p. 319–334.

Ortí, F., Helvaci, C., Rosell, L., and Gündogan, I., 1998, Sulphate–borate relations in an evaporitic lacustrine environment: the Sultançayir Gypsum (Miocene, western Anatolia): Sedimentology, v. 45, p. 697–710.

Palmer, M.R., and Helvaci, C., 1995, The boron geochemistry of the Kirka borate deposits, western Turkey: Geochimica et Cosmochimica Acta, v. 59, p. 3599–3605.

Rusansky, J.E., 1985, Estudio geológico–económico de la mina de boratos Santa Rosa 1 y 2, Depto. Los Andes, Salta [doctoral thesis]: Universidad Nacional de La Plata, Facultad de Ciencias Naturales y Museo, Argentina, p. 1–318.

Shearman, D.J., 1966, Origin of evaporites by diagenesis: Institution of Mining and Metallurgy, Transactions, Sect. B, v. 75, p. 208–215.

Shearman, D.J., Mossop, G., Dunsmore, H., and Martin, M., 1972, Origin of gypsum veins by hydraulic fracture: Institution of Mining and Metallurgy, Transactions, Sect. B, v. 81, p. 149–155.

Smith, G.I., 1985, Borate deposits in the United States: dissimilar in form, similar in geologic setting, *in* Barker, J.M., and Lefond, S.L., eds., Borates: Economic Geology and Production: New York, Society of Mining Engineers, p. 37–51.

Smith, G.I., and Medrano, M.D., 1996, Continental borate deposits of Cenozoic age, *in* Grew, E.S., and Anovitz, L.M., eds., Boron: Mineralogy, Petrology and Geochemistry: American Mineralogical Society, Reviews in Mineralogy, v. 33, p. 263–298.

Sun, D., and Li, B., 1993, Origins of borates in the saline lakes of China: Amsterdam, Elsevier, Seventh Symposium on Salt, vol. 1, p. 177–193.

Vandervoort, D.S., 1993, Non-marine evaporite basin studies, Southern Puna Plateau, Central Andes [unpublished Ph.D. thesis]: Cornell University, p. 1–177.

Vandervoort, D.S., 1997, Stratigraphic response to saline lake-level fluctuations and the origin of cyclic nonmarine evaporite deposits: The Pleistocene Blanca Lila Formation, northwest Argentina: Geological Society of America, Bulletin, v. 109, p. 210–224.

Vandervoort, D.S., Jordan, T.E., Zeitler, P.K., and Alonso, R.N., 1995, Chronology of internal drainage development and uplift, southern Puna plateau, Argentine central Andes: Geology, v. 23, p. 145–148.

Received 24 March 1999; accepted 27 September 1999.